“OSCILAÇÕES TROPICAIS DE 40-50 E 25-30 DIAS APARECENDO EM MODELOS CLIMÁTICOS IDEALIZADOS E REALÍSTICOS DO GFDL E EM DADOS DO ECMWF”

Tropical 40–50- and 25–30-Day Oscillations Appearing in Realistic and Idealized GFDL Climate Models and the ECMWF Dataset

HAYASHI, Y. AND D.G. GOLDER, 1993: ***TROPICAL 40–50- AND 25–30-DAY OSCILLATIONS APPEARING IN REALISTIC AND IDEALIZED GFDL CLIMATE MODELS AND THE ECMWF DATASET***. J. ATMOS. SCI., 50, 464–494

BRUNA FERREIRA RAMIM

Divisão do artigo

1. Introdução
2. Revisão teóricadas oscilações intrasazonais
   a) Teoria da onda de gravidade viscosa
   b) Teoria da forçante térmica
   c) Teoria da forçante térmica aleatória
   d) Teoria do Wave-CISK
   e) Teoria da instabilidade da resposta evaporação-vento
3. Modelo e dados observados
4. Características das ondas
   a) Distribuição das frequências dos números de onda
   b) Distribuição longitudinal
   c) Distribuição temporal
5. Estrutura na escala planetária
   a) Padrões de onda
   b) Estrutura latitudinal
   c) Estrutura vertical
6. Efeitos de uma maior resolução vertical
7. Efeitos de variações geográficas e sazonais
   a) Oscilações na escala planetária
   b) Oscilações na escala supercluster
   c) Relação entre a precipitação e a velocidade vertical
   d) Propagação das oscilações da escala planetária e supercluster
8. Conclusões e observações

1. Introdução

- Hayashi a Golder (1986, 1988):
  - Estudo da propagação e estrutura das oscilações intrasazonais tropicais que apareciam no modelo (GFDL – *Geophysical Fluid Dynamics Laboratory*) e nas observações (FGGE – *First GARP (Global Atmospheric Research Program) Global Experiment*)
  - Truncamento romboidal R30 e R15
  - Diferenças nas amplitudes das oscilações modeladas e observadas: degradação da previsão de tempo

- Objetivo:
  - Diferenças entre as oscilações de 40-50 e 25-30 dias
  - Avaliar as simulações e teorias com os dados observados

- Metodologia:
  - 9 anos de dados do modelo R30 de nove níveis
  - Conjunto de dados da análise do ECMWF(1979-1987, incluindo o FGGE de 1979)
  - Efeitos de melhor resolução vertical: modelo SKYHI (40 níveis, do GFDL => GCM, diferenças finitas, troposfera-estratosfera-mesosfera)
  - Efeitos das remoções das variações geográficas e sazonais: modelo R30 superfície oceânica janeiro perpétuo

2. Revisão teórica das oscilações intrasazonais

a) Teoria da onda de gravidade viscosa
   - Chang (1977): o comprimento de onda vertical esperado na teoria pode ser modificado para o valor observado pelo efeito da forte viscosidade devido ao transporte de momento pelos cumulus

b) Teoria da forçante térmica
   - Yamagata e Hayashi (1984): forçante térmica oscilando e produzindo oscilações intrasazonais; combinação Kelvin (p/ leste da forçante) e Rossby (p/ oeste da forçante) => identificação no modelo e nos dados (mas com propagação para leste)
   - Hayashi e Miyahara (1987): amplitude do mov. para leste modulada geograficamente
   - A propagação para leste é resultado global ou local da propagação para leste do aquecimento?

c) Teoria da forçante térmica aleatória
   - Escala vertical da forçante

d) Teoria do Wave-CISK
   - Efeito médio do aquecimento dos cumulus é proporcional a convergência de umidade na camada superficial

e) Teoria da instabilidade da resposta evaporação-vento
   - O aquecimento convectivo é proporcional também a evaporação (não só a convergência de umidade), que é proporcional ao vento em superficie

3. Modelo e dados observados

- Modelo: GFDL (9 níveis) R30
- Dados “observados”: modelo integrado por 9 anos (dezembro de 1978 a novembro de 1979 (ano do FGGE) e janeiro de 1980 a dezembro de 1987 ⇔ dados FGGE são os dados do ECMWF para o ano do FGGE)

4. Características das ondas

a) Distribuição das frequências dos números de onda

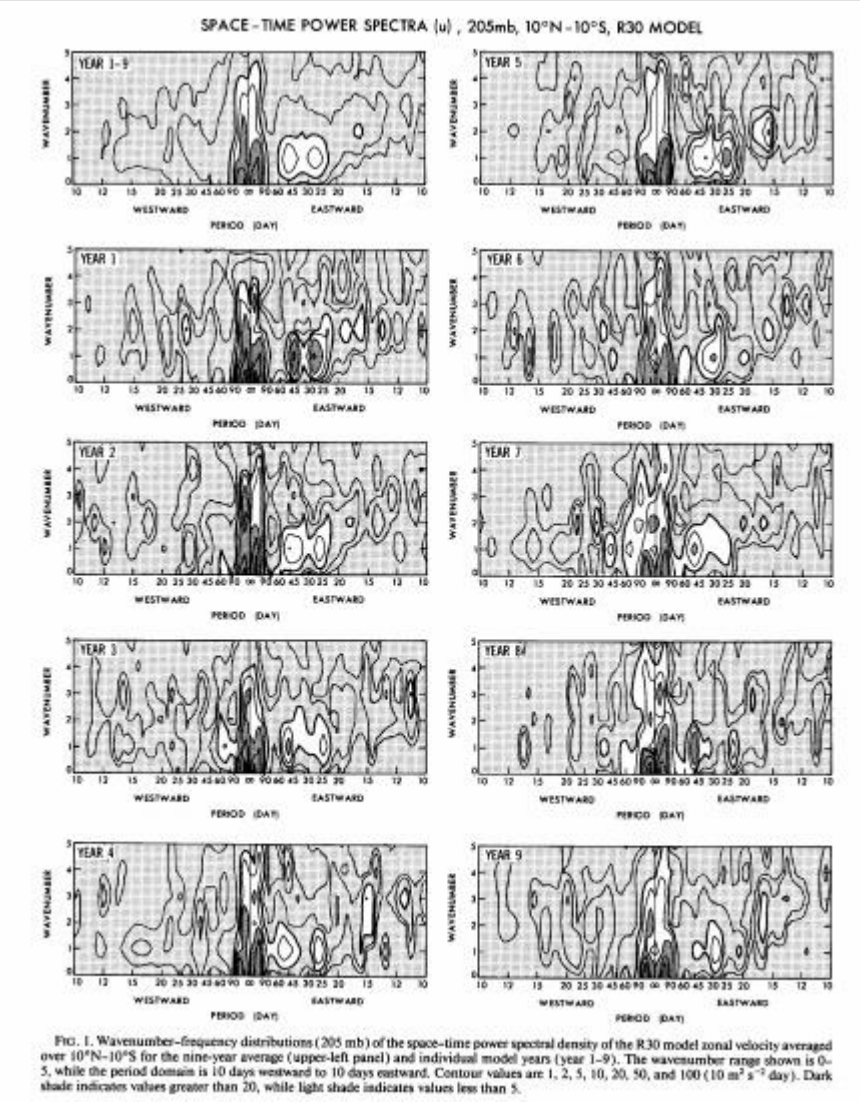

FIG. 1. Wavenumber–frequency distributions (205 mb) of the space–time power spectral density of the R30 model zonal velocity averaged over 10°N–10°S for the nine-year average (upper-left panel) and individual model years (year 1–9). The wavenumber range shown is 0–5, while the period domain is 10 days westward to 10 days eastward. Contour values are 1, 2, 5, 10, 20, 50, and 100 ($10\ m^2\ s^{-2}$ day). Dark shade indicates values greater than 20, while light shade indicates values less than 5.

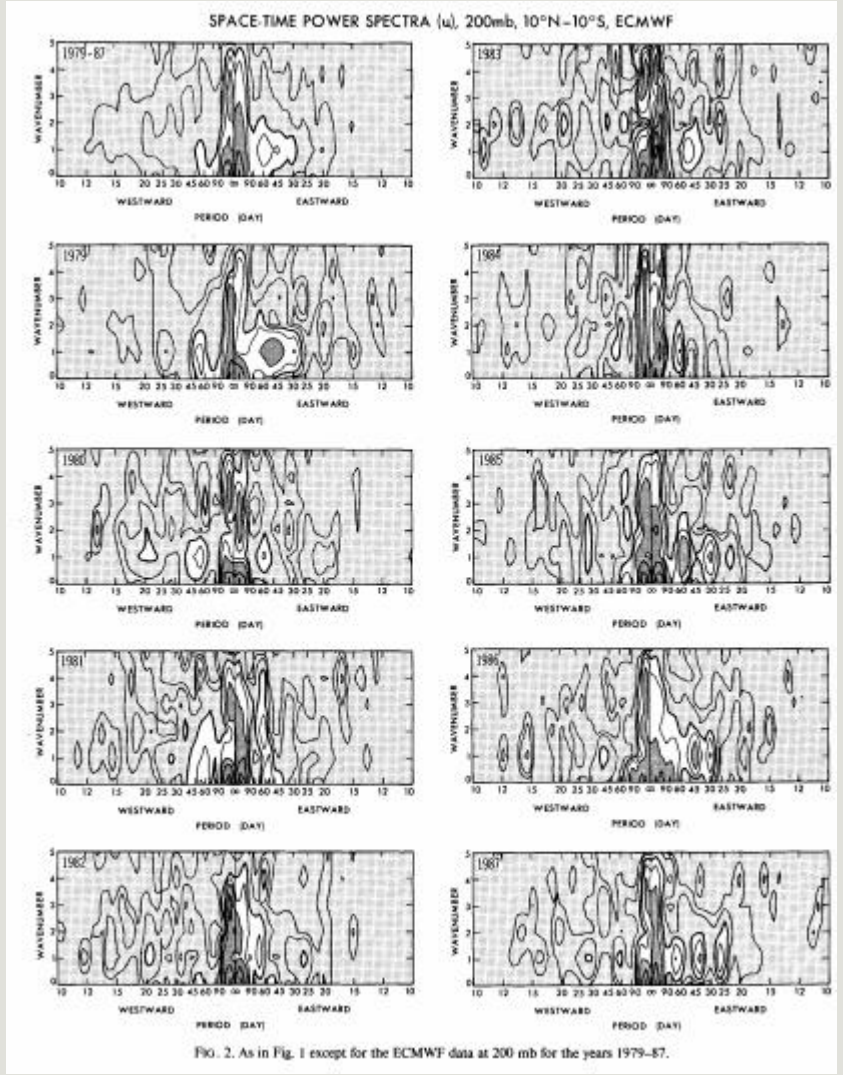

FIG. 2. As in Fig. 1 except for the ECMWF data at 200 mb for the years 1979–87.

4. Características das ondas

Média latitudinal

a) Distribuição das frequências dos números de onda

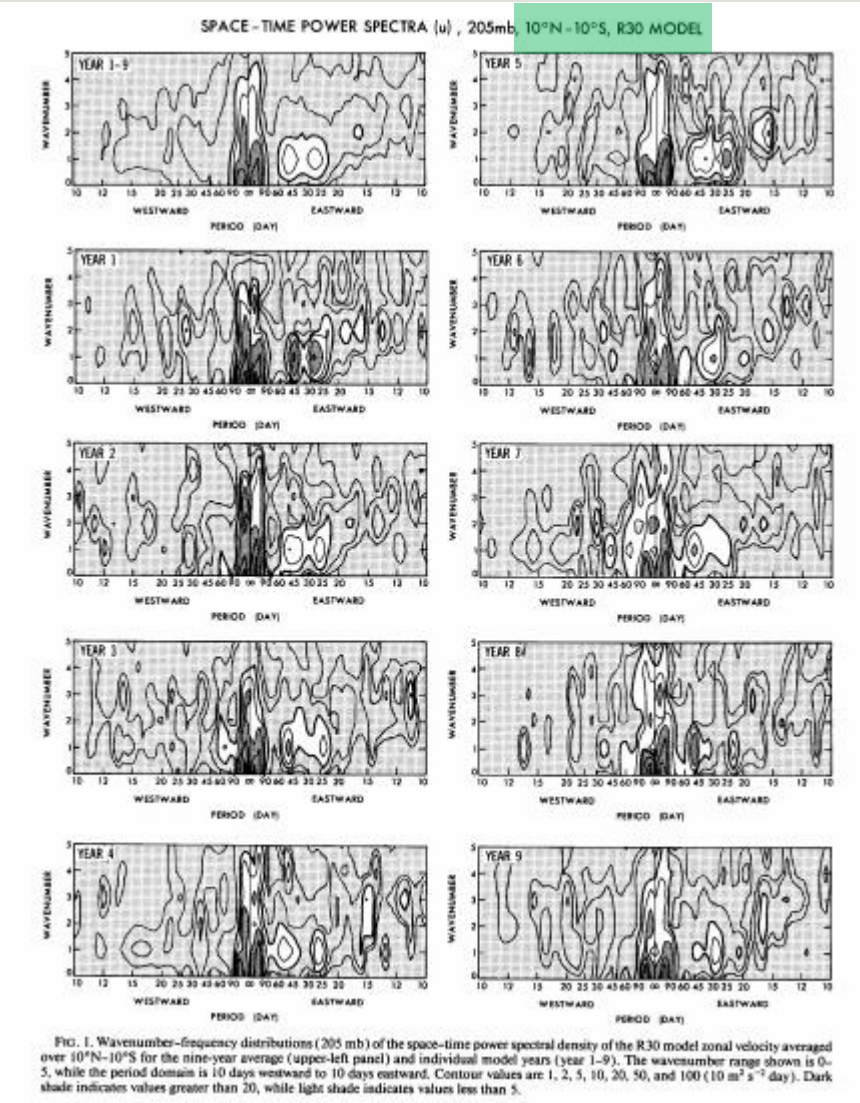

FIG. 1. Wavenumber–frequency distributions (205 mb) of the space–time power spectral density of the R30 model zonal velocity averaged over 10°N–10°S for the nine-year average (upper-left panel) and individual model years (year 1–9). The wavenumber range shown is 0–5, while the period domain is 10 days westward to 10 days eastward. Contour values are 1, 2, 5, 10, 20, 50, and 100 ($10\ m^2\ s^{-2}$ day). Dark shade indicates values greater than 20, while light shade indicates values less than 5.

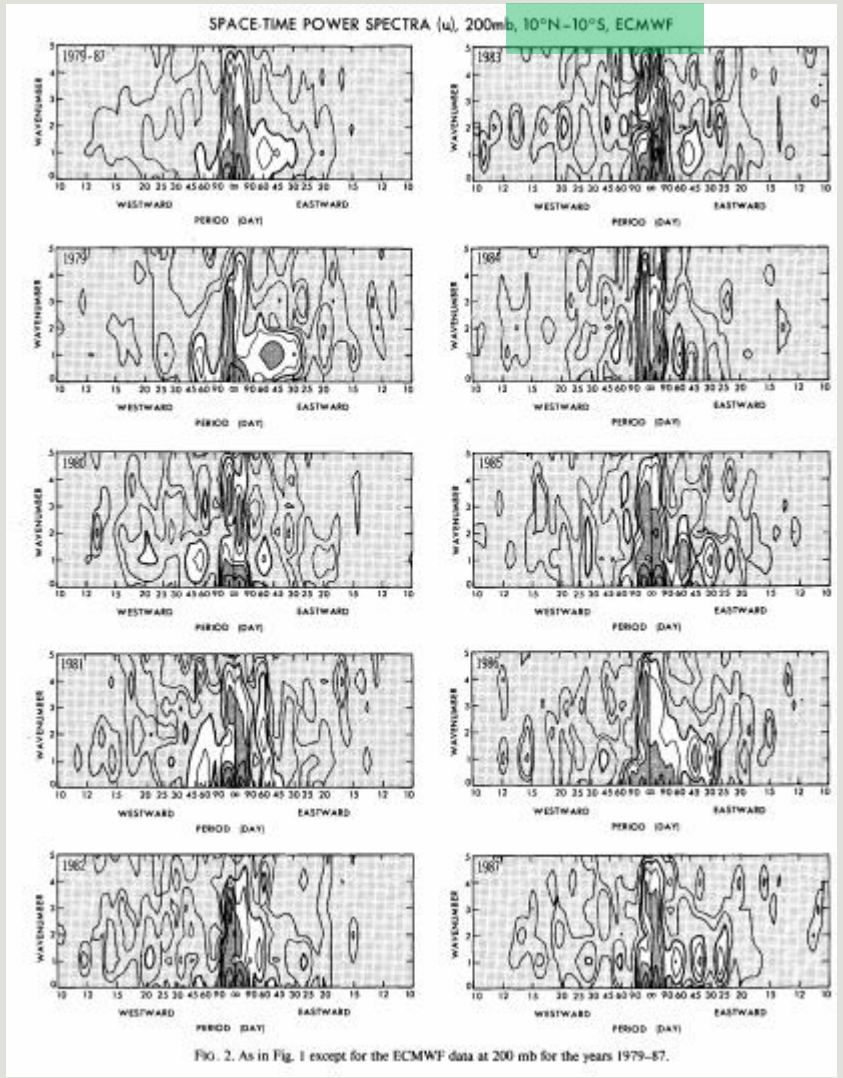

FIG. 2. As in Fig. 1 except for the ECMWF data at 200 mb for the years 1979–87.

4. Características das ondas

Média 9 anos

a) Distribuição das frequências dos números de onda

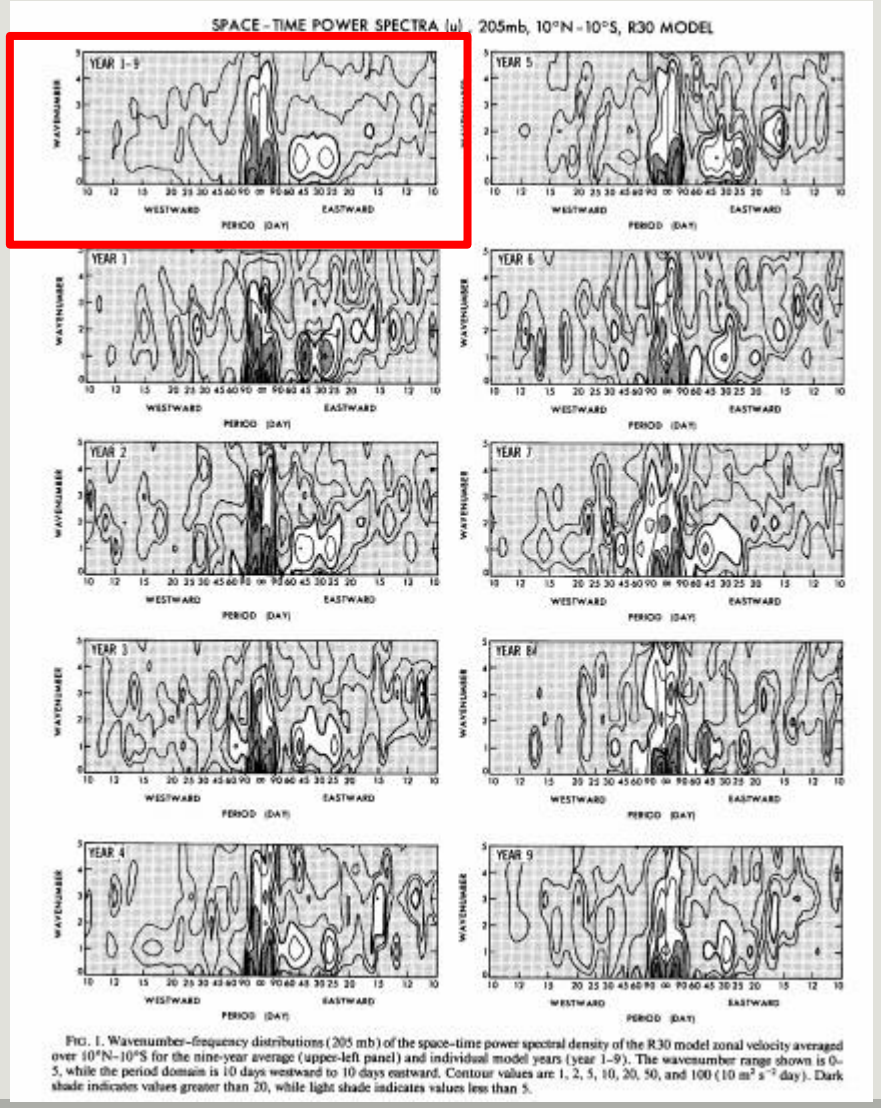

FIG. 1. Wavenumber–frequency distributions (205 mb) of the space–time power spectral density of the R30 model zonal velocity averaged over 10°N–10°S for the nine-year average (upper-left panel) and individual model years (year 1–9). The wavenumber range shown is 0–5, while the period domain is 10 days westward to 10 days eastward. Contour values are 1, 2, 5, 10, 20, 50, and 100 ($10\ m^2\ s^{-2}$ day). Dark shade indicates values greater than 20, while light shade indicates values less than 5.

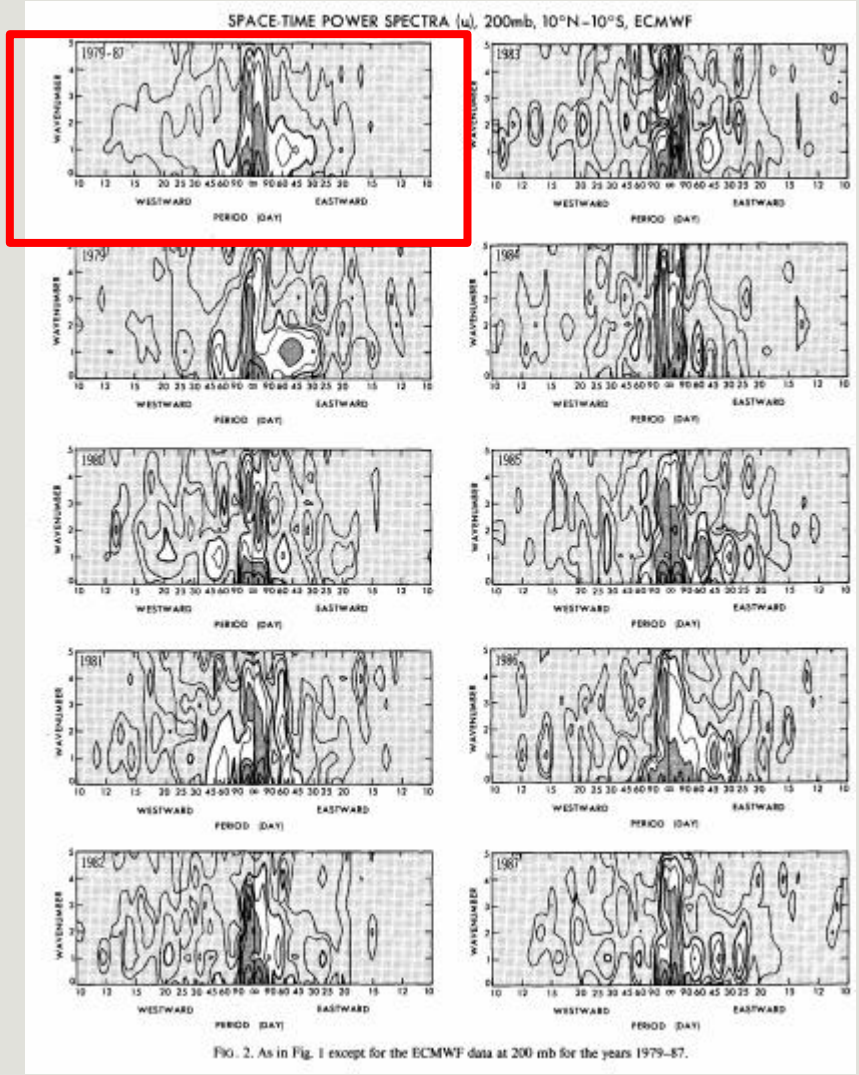

FIG. 2. As in Fig. 1 except for the ECMWF data at 200 mb for the years 1979–87.

4. Características das ondas

a) Distribuição das frequências dos números de onda

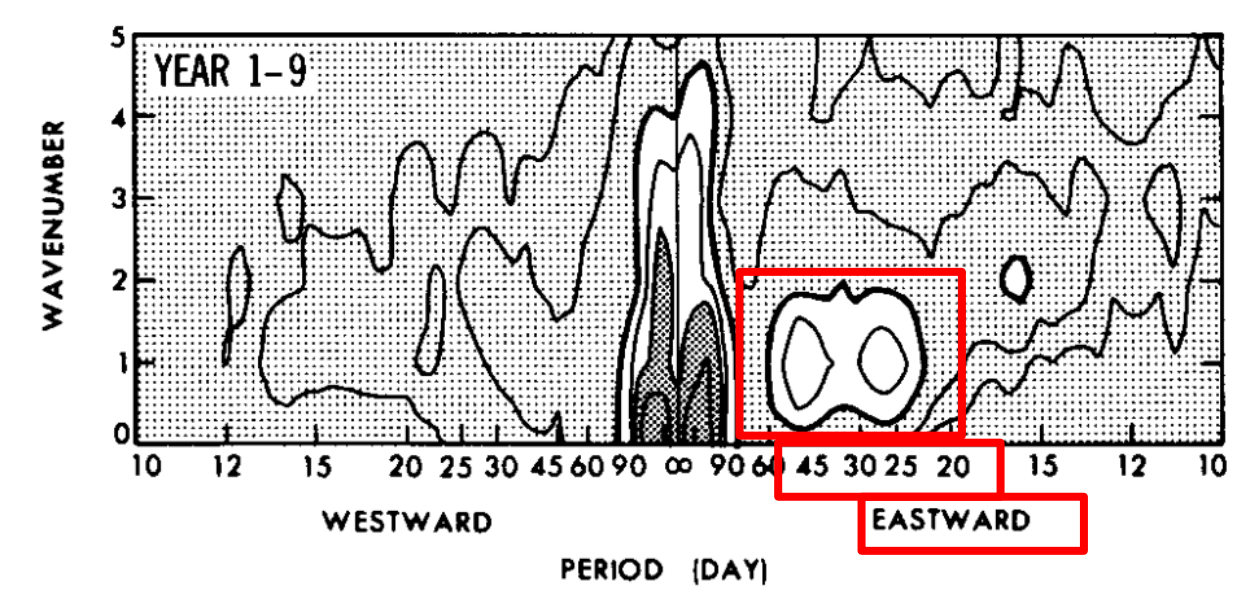

4. Características das ondas

a) Distribuição das frequências dos números de onda

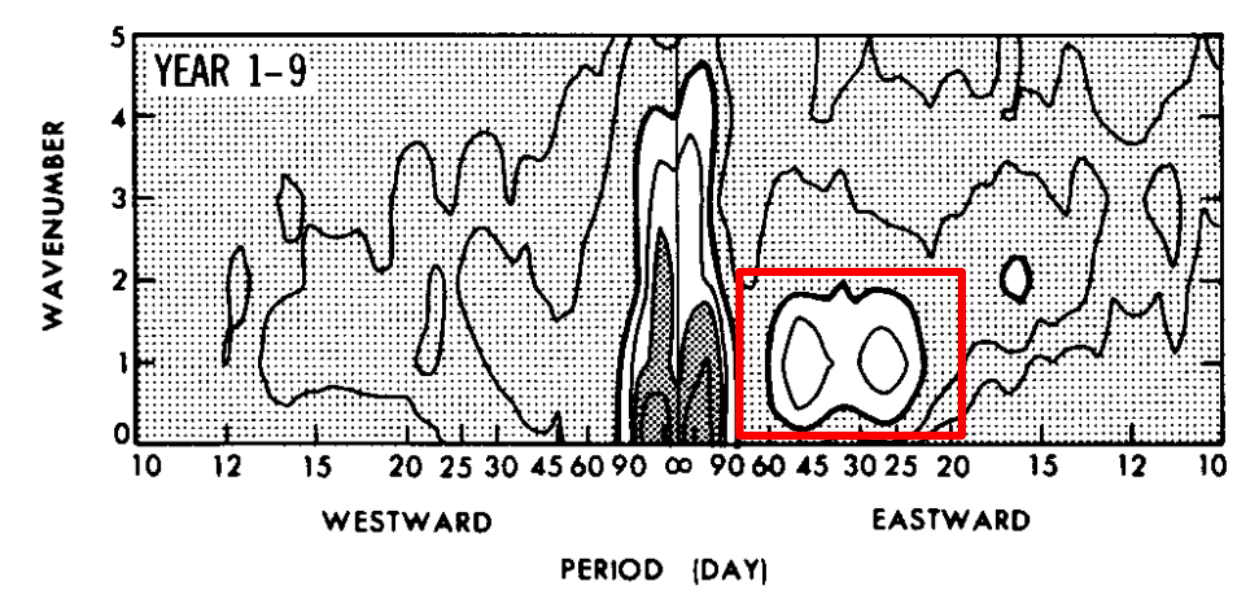

Dois picos com magnitudes semelhantes

Dois picos, com uma magnitude dominante

Um pico

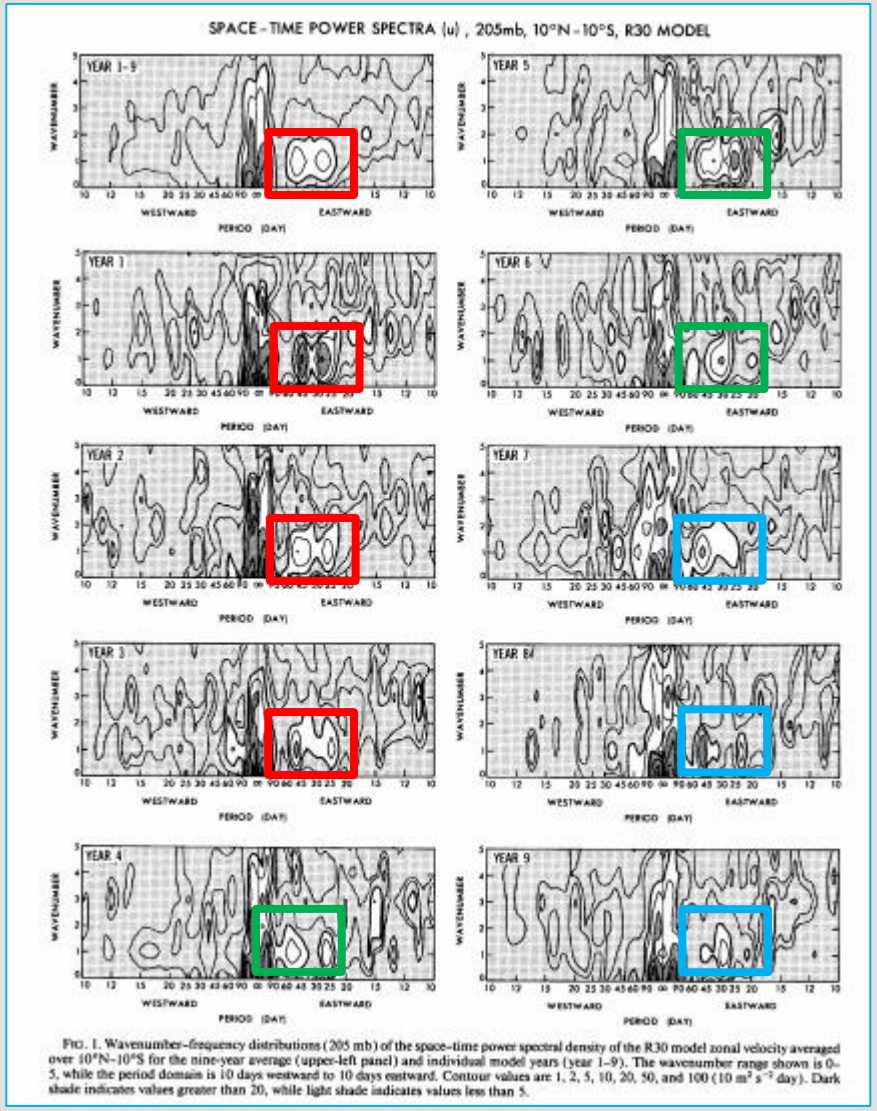

FIG. 1. Wavenumber–frequency distributions (205 mb) of the space–time power spectral density of the R30 model zonal velocity averaged over 10°N–10°S for the nine-year average (upper-left panel) and individual model years (year 1–9). The wavenumber range shown is 0–5, while the period domain is 10 days westward to 10 days eastward. Contour values are 1, 2, 5, 10, 20, 50, and 100 ($10\ m^2\ s^{-2}$ day). Dark shade indicates values greater than 20, while light shade indicates values less than 5.

4. Características das ondas

a) Distribuição das frequências dos números de onda

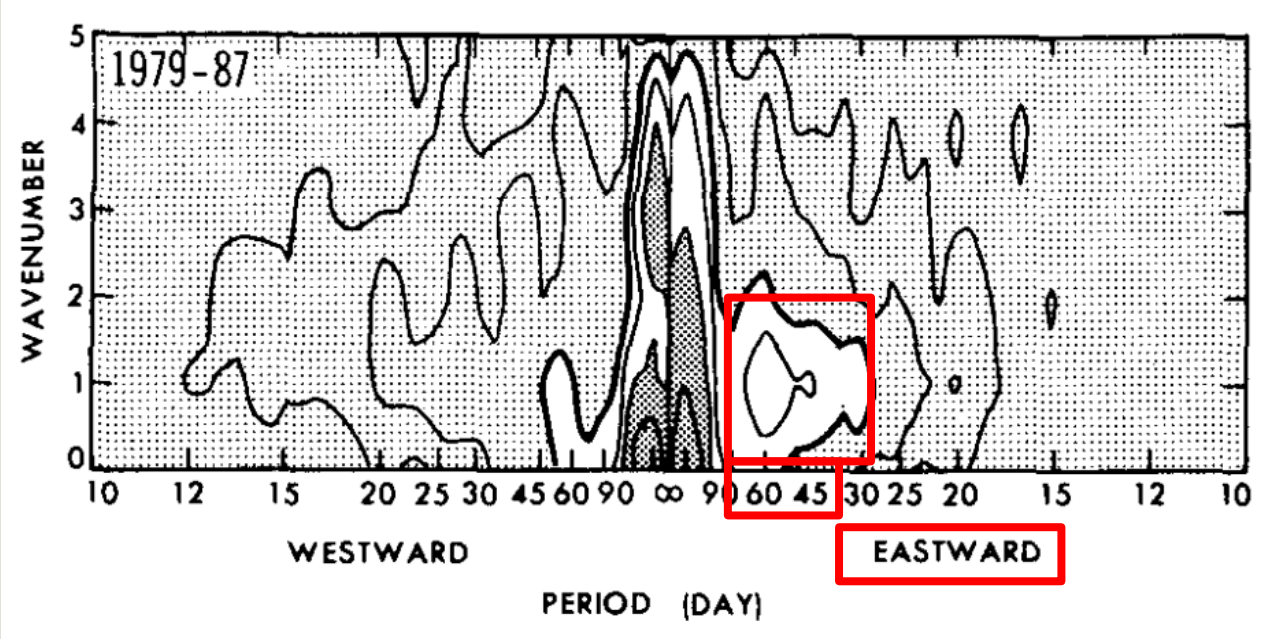

Comparável com o modelado

4. Características das ondas

a) Distribuição das frequências dos números de onda

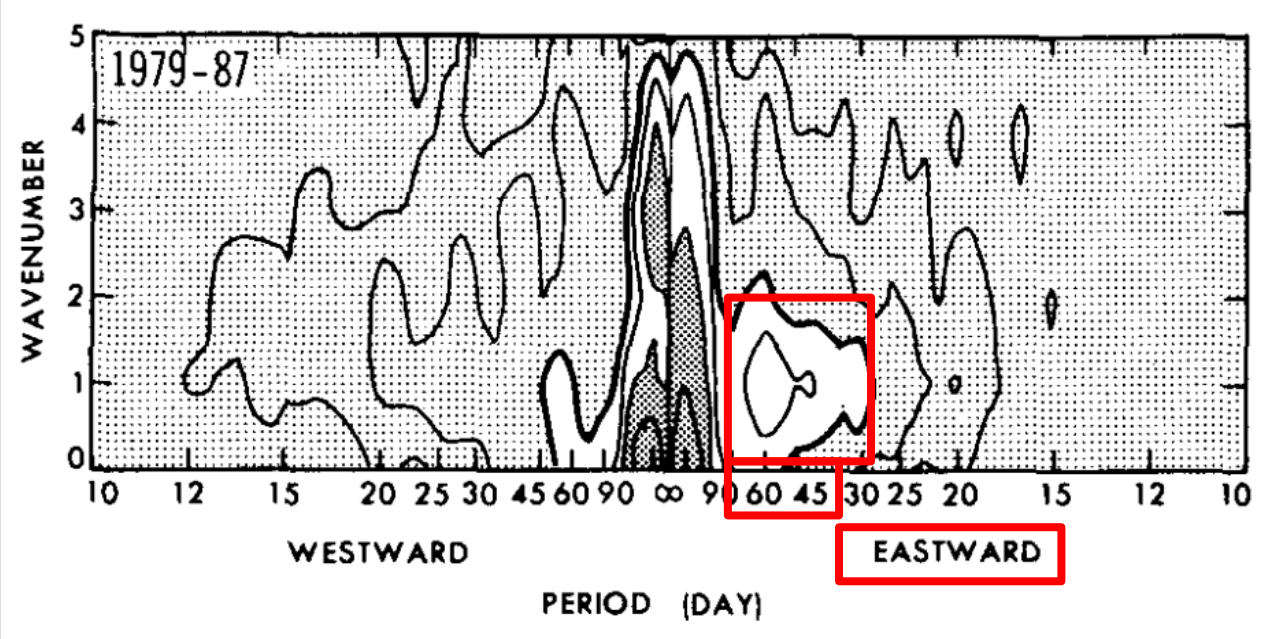

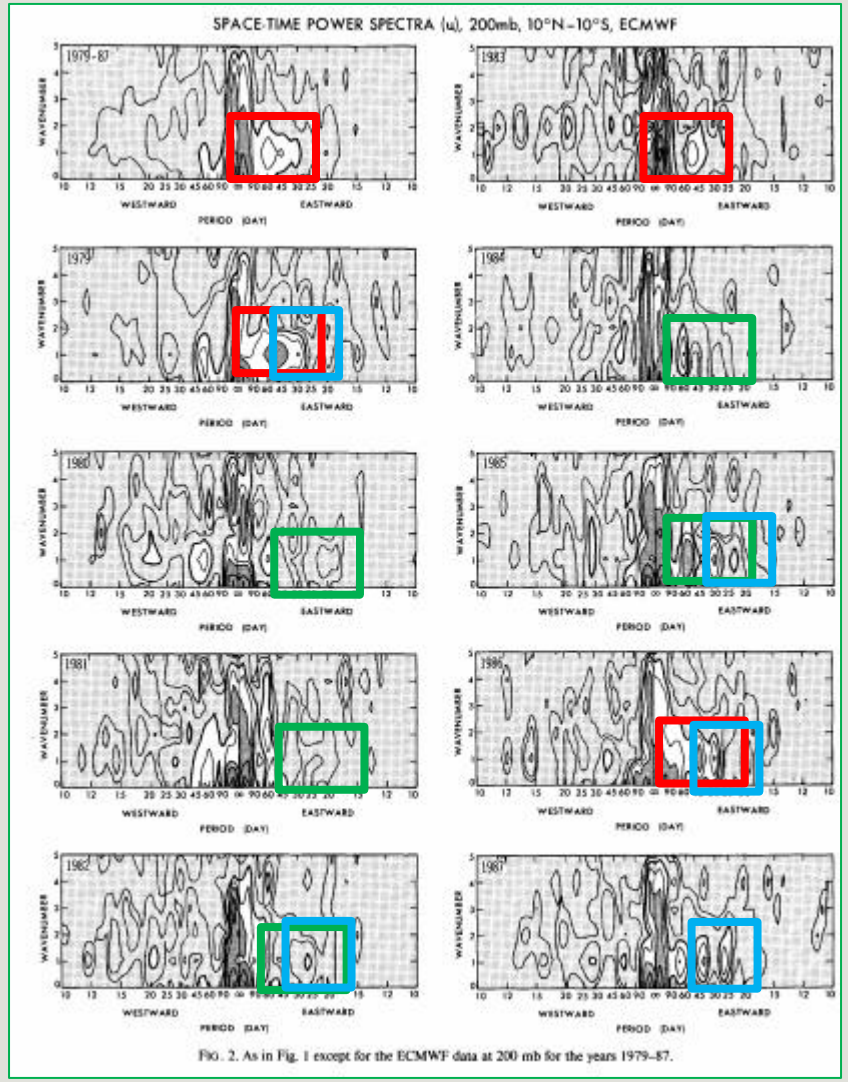

Fig. 2. As in Fig. 1 except for the ECMWF data at 200 mb for the years 1979–87.

Pico ~40-50 dias

Pico ~50-60 dias

Pico ~25-30 dias

4. Características das ondas

a) Distribuição das frequências dos números de onda
   - ECMWF apresenta uma variabilidade interanual mais forte que o modelo R30, que não tem variabilidade interanual na TSM

4. Características das ondas

a) Distribuição das frequências dos números de onda

* Variação sazonal removida

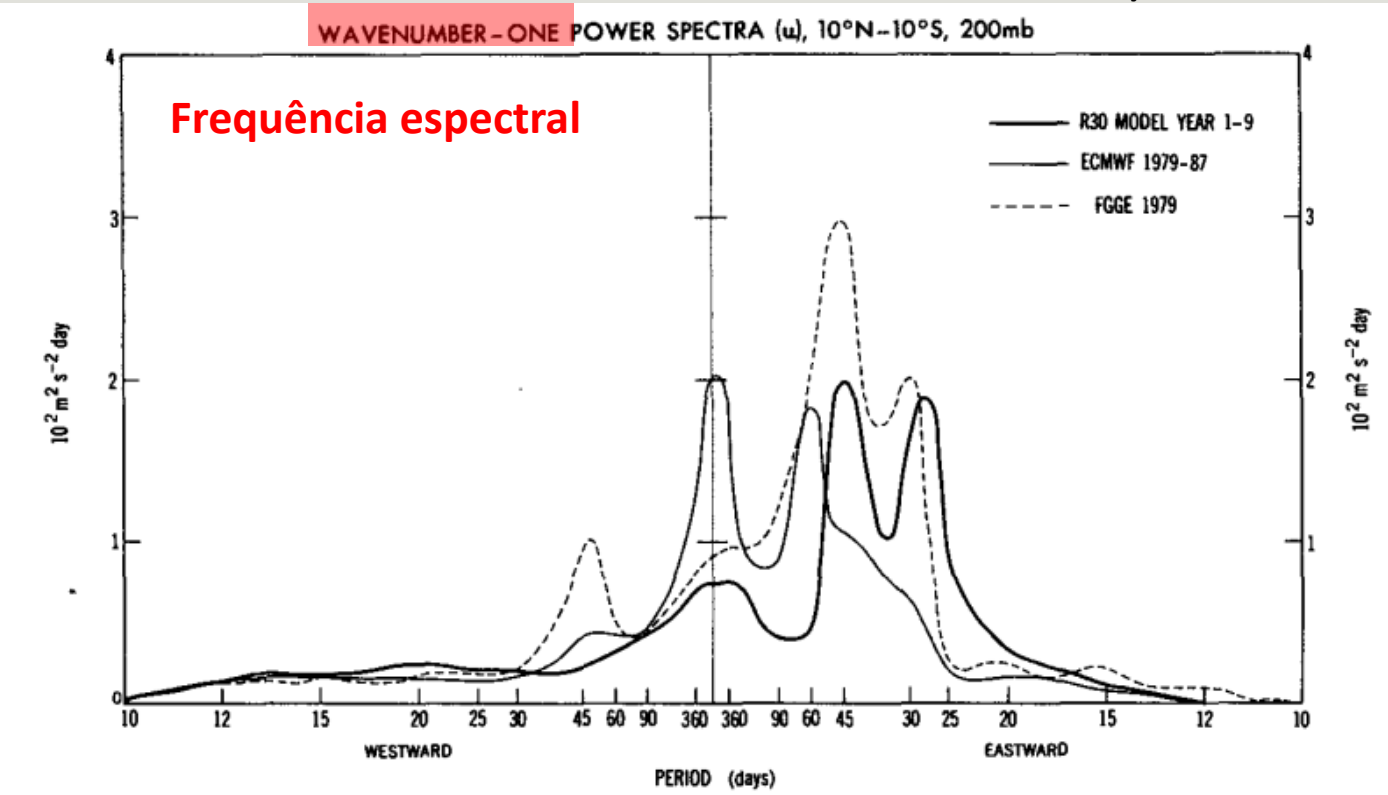

FIG. 3. Frequency–spectral distribution of the wavenumber-1 component space–time power spectral density (100 m^2 s^{-2} day) of zonal velocity averaged over 10°N–10°S for the R30 model at 205 mb, year 1–9 (thick curve), the ECMWF data at 200 mb, 1979–87 (thin curve), and the FGGE data at 200 mb, 1979 (dashed curve). Seasonal variations were removed prior to the spectral analysis.

4. Características das ondas

a) Distribuição das frequências dos números de onda

* Variação sazonal removida

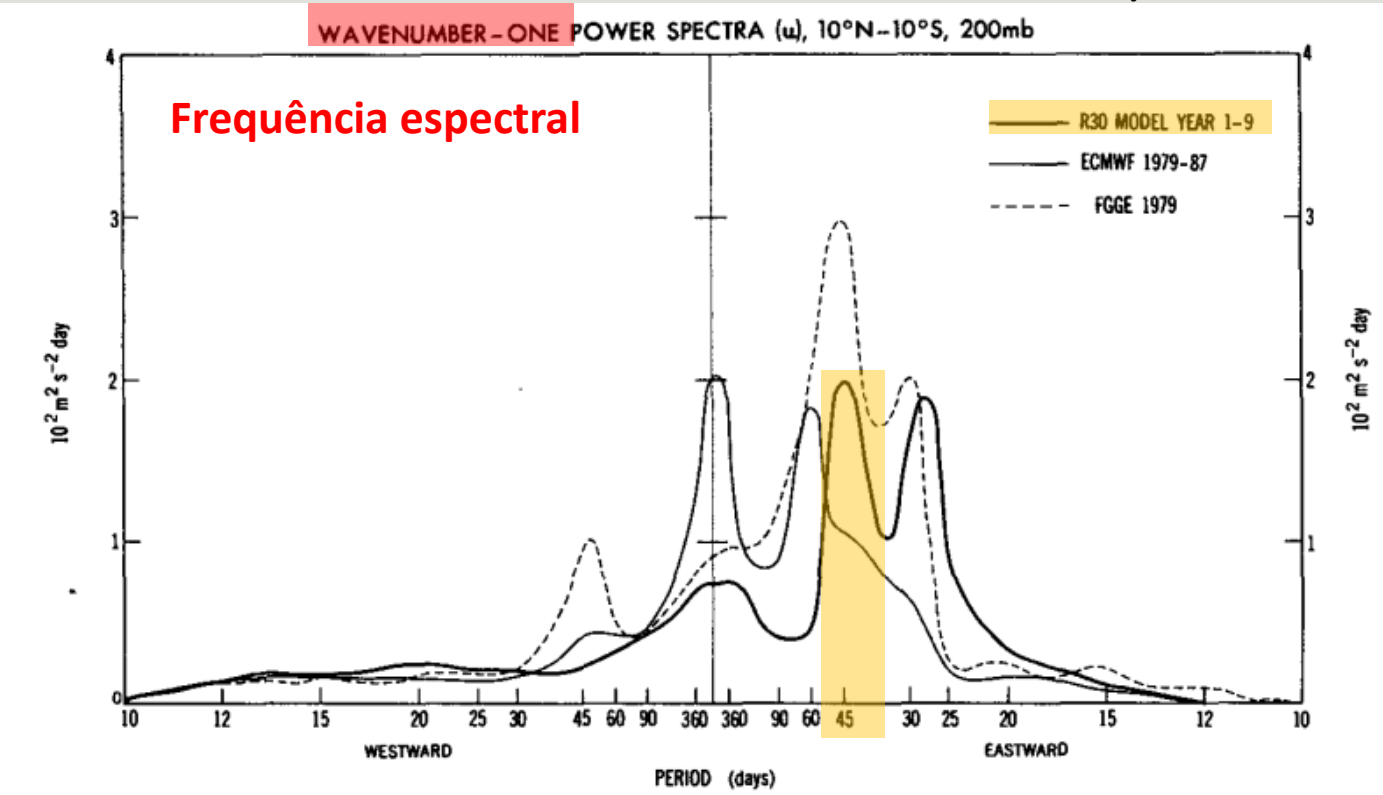

FIG. 3. Frequency–spectral distribution of the wavenumber-1 component space–time power spectral density (100 m^2 s^{-2} day) of zonal velocity averaged over 10°N–10°S for the R30 model at 205 mb, year 1–9 (thick curve), the ECMWF data at 200 mb, 1979–87 (thin curve), and the FGGE data at 200 mb, 1979 (dashed curve). Seasonal variations were removed prior to the spectral analysis.

4. Características das ondas

a) Distribuição das frequências dos números de onda

* Variação sazonal removida

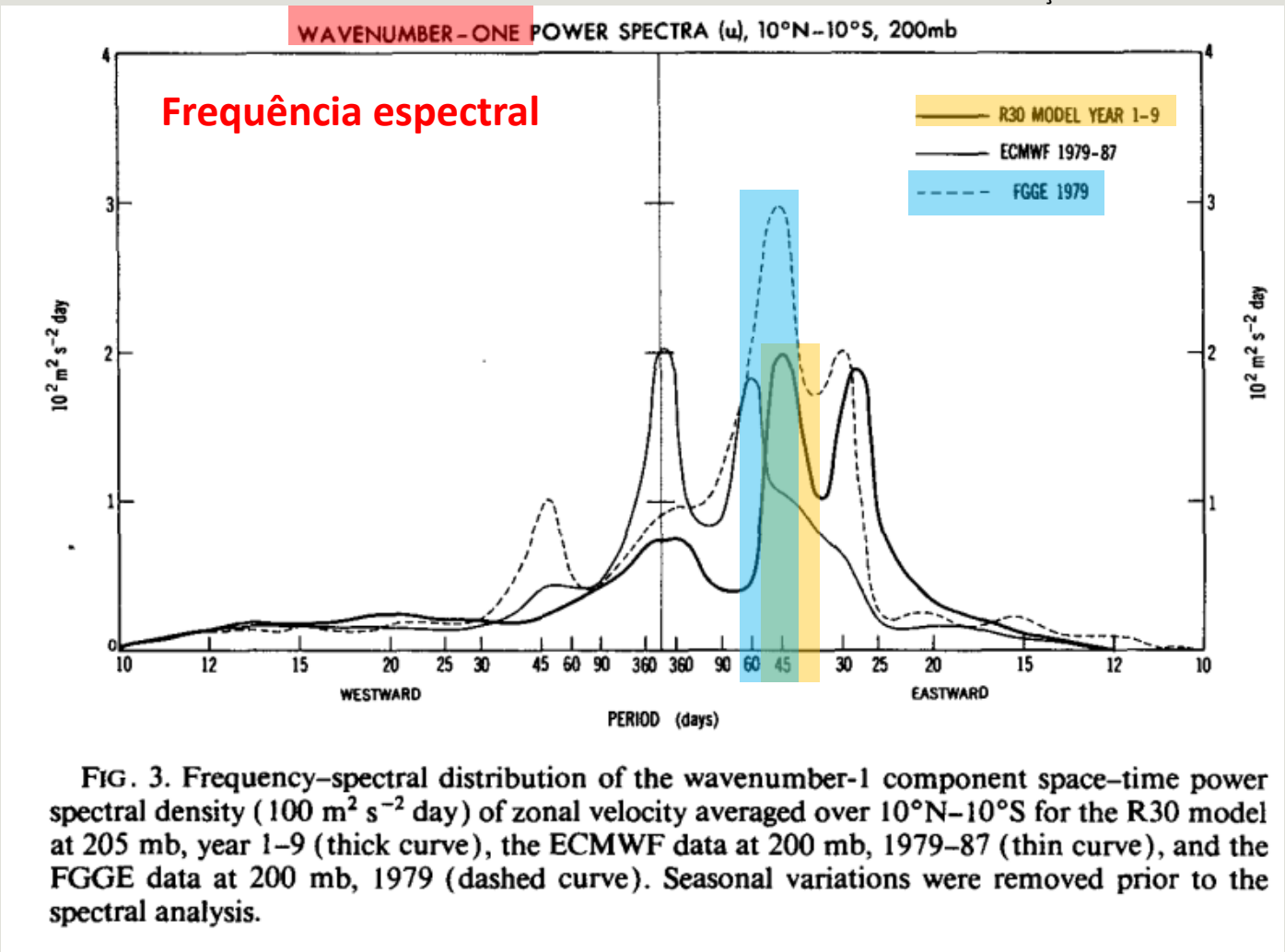

FIG. 3. Frequency–spectral distribution of the wavenumber-1 component space–time power spectral density (100 m^2 s^{-2} day) of zonal velocity averaged over 10°N–10°S for the R30 model at 205 mb, year 1–9 (thick curve), the ECMWF data at 200 mb, 1979–87 (thin curve), and the FGGE data at 200 mb, 1979 (dashed curve). Seasonal variations were removed prior to the spectral analysis.

Mais fraco

4. Características das ondas

a) Distribuição das frequências dos números de onda

* Variação sazonal removida

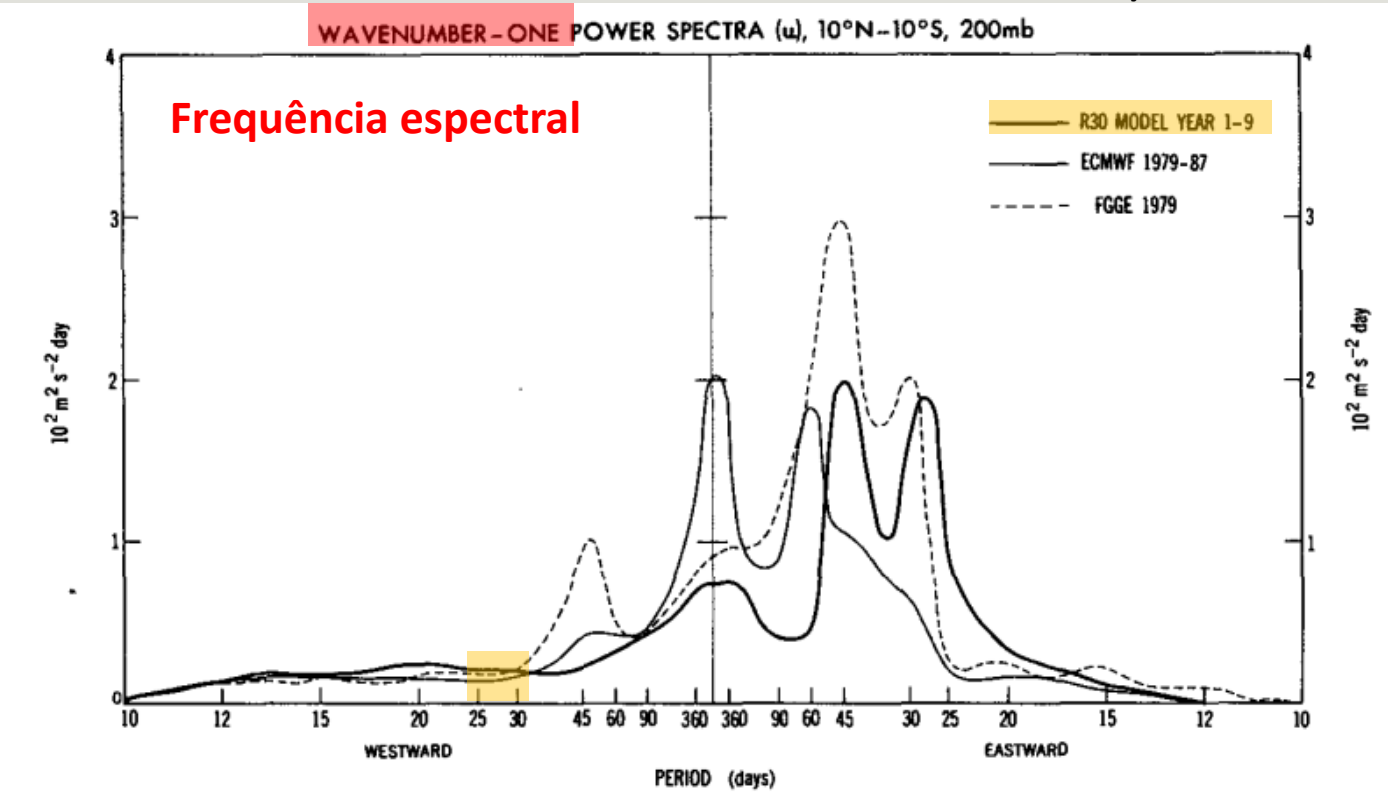

FIG. 3. Frequency–spectral distribution of the wavenumber-1 component space–time power spectral density (100 m^2 s^{-2} day) of zonal velocity averaged over 10°N–10°S for the R30 model at 205 mb, year 1–9 (thick curve), the ECMWF data at 200 mb, 1979–87 (thin curve), and the FGGE data at 200 mb, 1979 (dashed curve). Seasonal variations were removed prior to the spectral analysis.

4. Características das ondas

a) Distribuição das frequências dos números de onda

* Variação sazonal removida

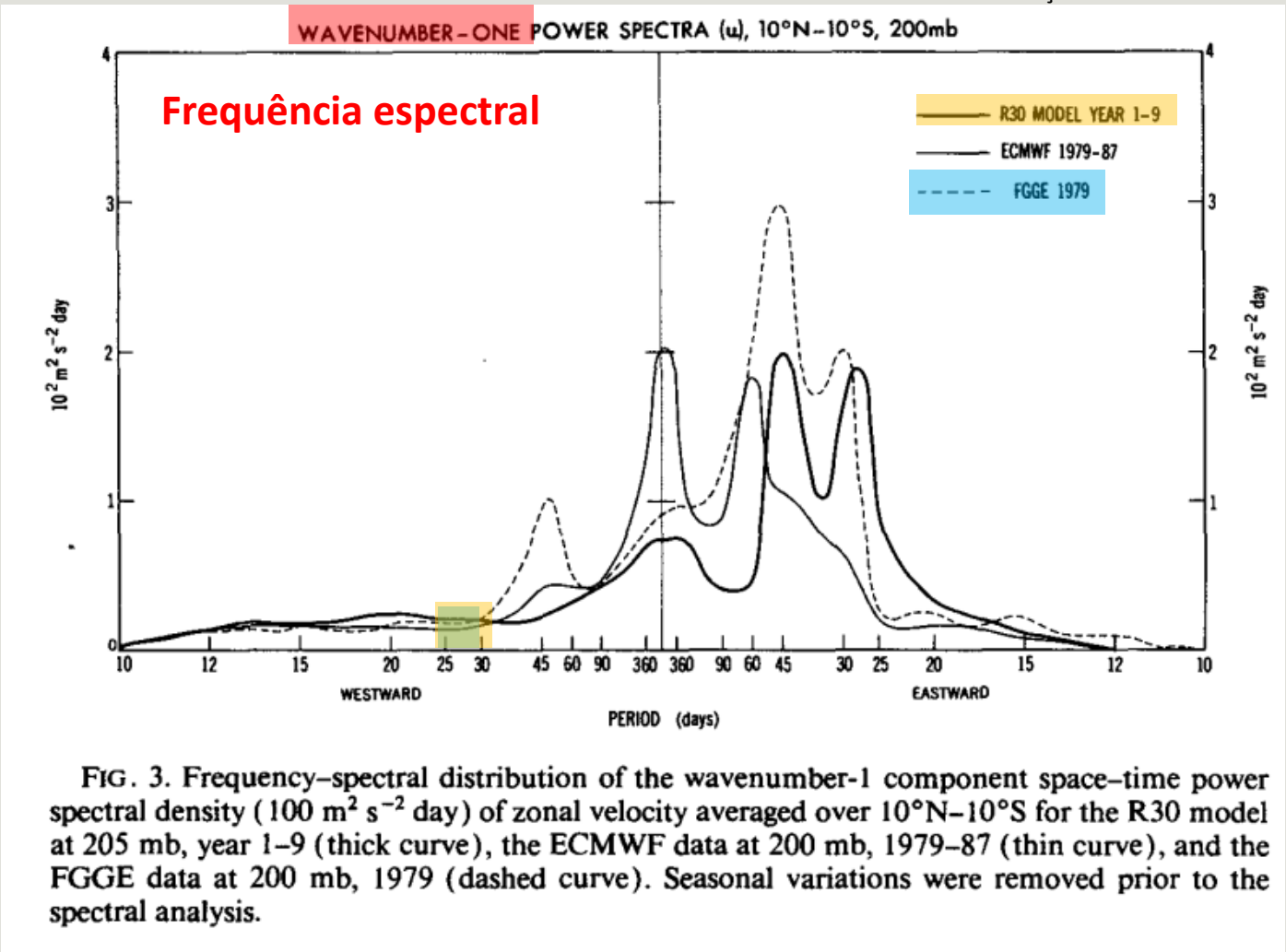

FIG. 3. Frequency–spectral distribution of the wavenumber-1 component space–time power spectral density (100 m^2 s^{-2} day) of zonal velocity averaged over 10°N–10°S for the R30 model at 205 mb, year 1–9 (thick curve), the ECMWF data at 200 mb, 1979–87 (thin curve), and the FGGE data at 200 mb, 1979 (dashed curve). Seasonal variations were removed prior to the spectral analysis.

Similares

b) Distribuição longitudinal

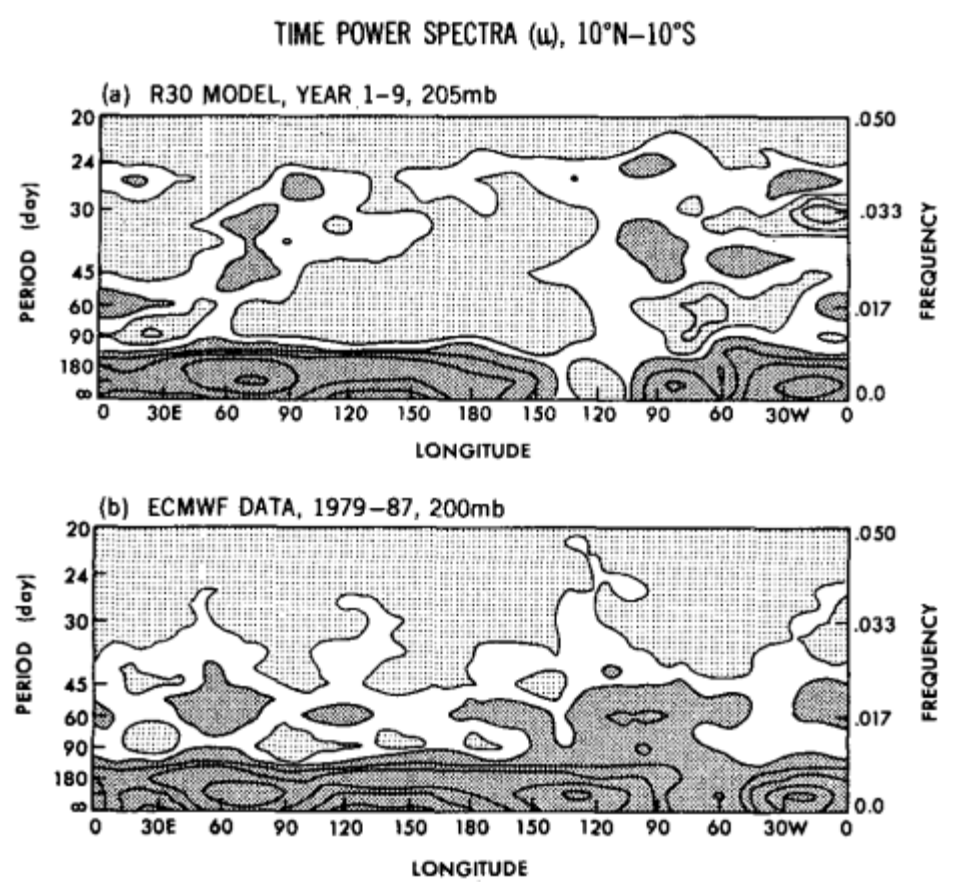

FIG. 4. Longitude–frequency distributions of the time-power spectral density (year 1–9) of the zonal velocity averaged between 10°N–10°S of the R30 model (a) at 205 mb and the ECMWF data 1979–87 (b) at 200 mb. Contours 20, 50, 100, 200, 500, and 1000 (10 $m^2 s^{-2}$ day). Dark shade > 50, light shade < 20.

Período de 40-50 ou 25-30 dias: velocidades de fase localmente distintas (dependendo da média local do escoamento)

b) Distribuição longitudinal

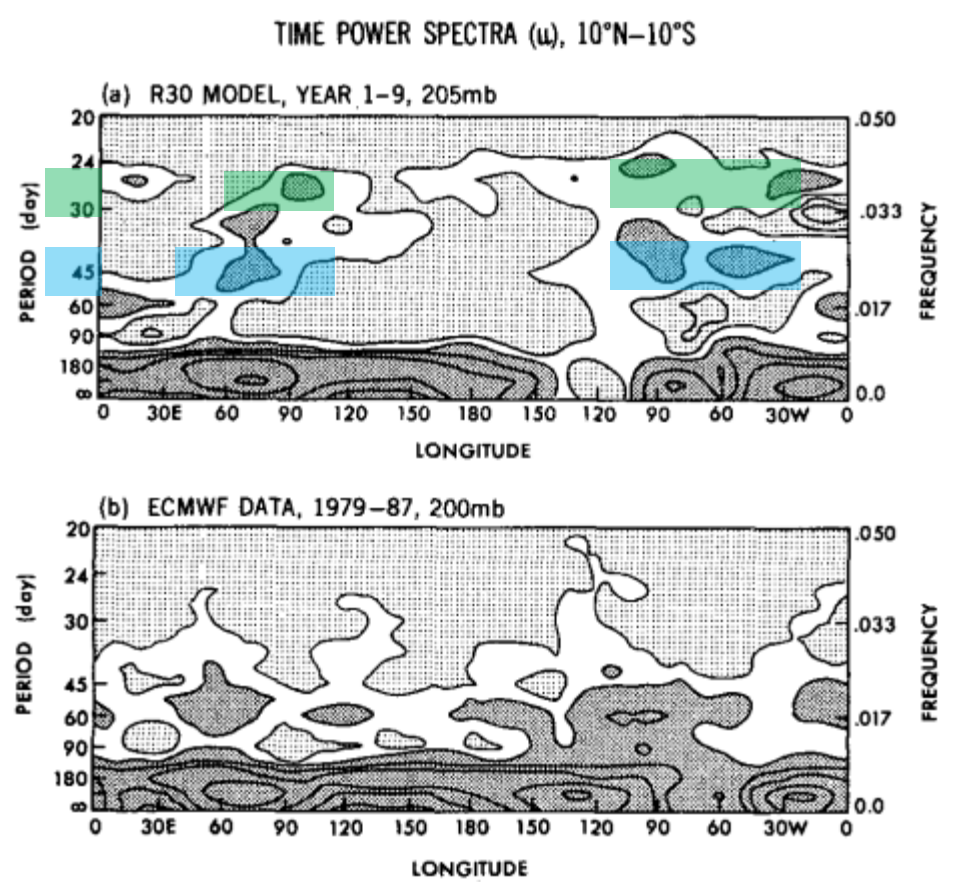

FIG. 4. Longitude–frequency distributions of the time-power spectral density (year 1–9) of the zonal velocity averaged between 10°N–10°S of the R30 model (a) at 205 mb and the ECMWF data 1979–87 (b) at 200 mb. Contours 20, 50, 100, 200, 500, and 1000 (10 $m^2 s^{-2}$ day). Dark shade > 50, light shade < 20.

Período de 40-50 ou 25-30 dias: velocidades de fase localmente distintas (dependendo da média local do escoamento)

De região pra região os períodos não variam muito ⇔ oscilações não são isoladas longitudinalmente

b) Distribuição longitudinal

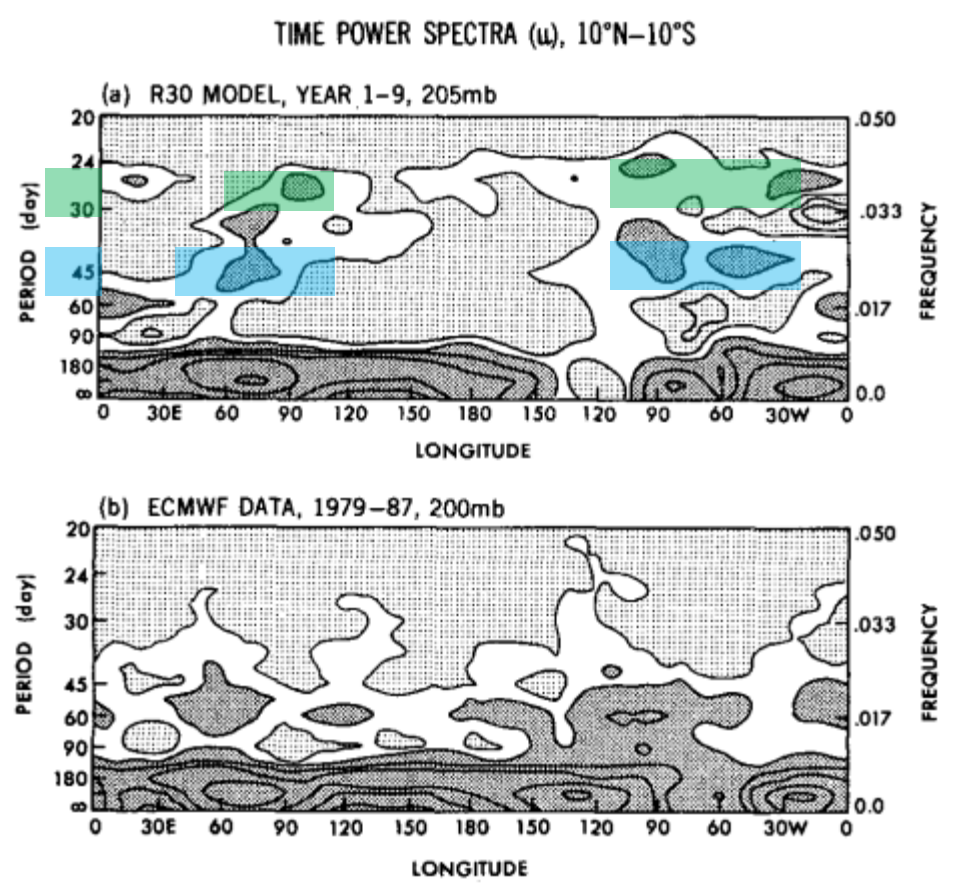

FIG. 4. Longitude–frequency distributions of the time-power spectral density (year 1–9) of the zonal velocity averaged between 10°N–10°S of the R30 model (a) at 205 mb and the ECMWF data 1979–87 (b) at 200 mb. Contours 20, 50, 100, 200, 500, and 1000 (10 $m^2 s^{-2}$ day). Dark shade > 50, light shade < 20.

Período de 40-50 ou 25-30 dias: velocidades de fase localmente distintas (dependendo da média local do escoamento)

De região pra região os períodos não variam muito ⇔ oscilações não são isoladas longitudinalmente

Comportamento parecido nos dados observados

c) Distribuição temporal

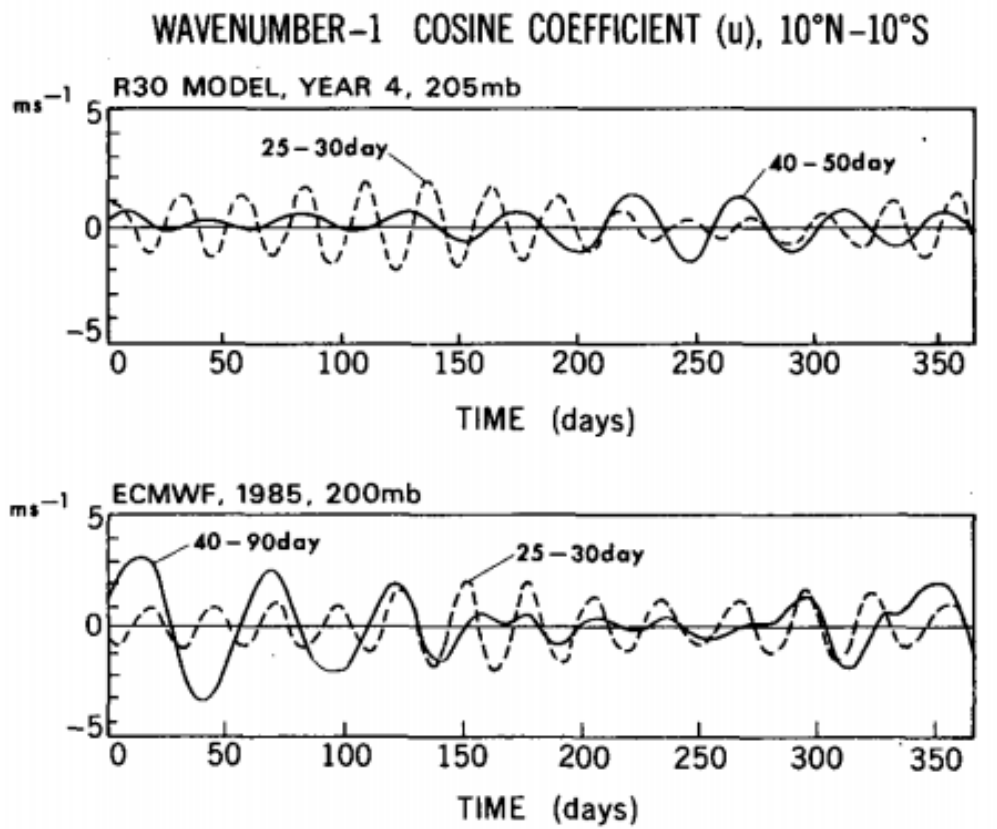

FIG. 5. Time distribution of the frequency-filtered wavenumber-one cosine coefficient (m s^{-1}) of zonal velocity averaged between 10°N–10°S. The upper panel represents the R30 model (year 4) at 205 mb, 40–50-day filtered (solid curve) and 25–30-day filtered (dashed curve). The lower panel represents the ECMWF data (1985) at 200 mb, 40–90-day filtered (solid curve) and 25–30-day filtered (dashed curve).

Período de 40-50 ou 25-30 dias: velocidades de fase localmente distintas (dependendo da variação sazonal do fluxo zonal)

Oscilações de 40-50 ou 25-30 dias: aparecem fortemente durante diferentes estações do ano

5. Estrutura na escala planetária

a) Padrões de onda
   - Oscilações intrasazonais são associadas com 3 estruturas:
     - ✓ Planetária (propaga globalmente => nº de onda 1)
     - ✓ Supercluster (velocidade vertical concentrada propagando globalmente => nº de onda 5-10)
     - ✓ Regional (depende da localização; numerosos nº de onda)

Perto do Equador: mov. para leste exibe padrão de Kelvin (vetores de vento direcionados paralelamente para o EQ; comp. zonal em fase com a altura geopotencial)

Longe do Equador: Rossby (vetores de vento direcionados ao longo do campo de geopotencial)

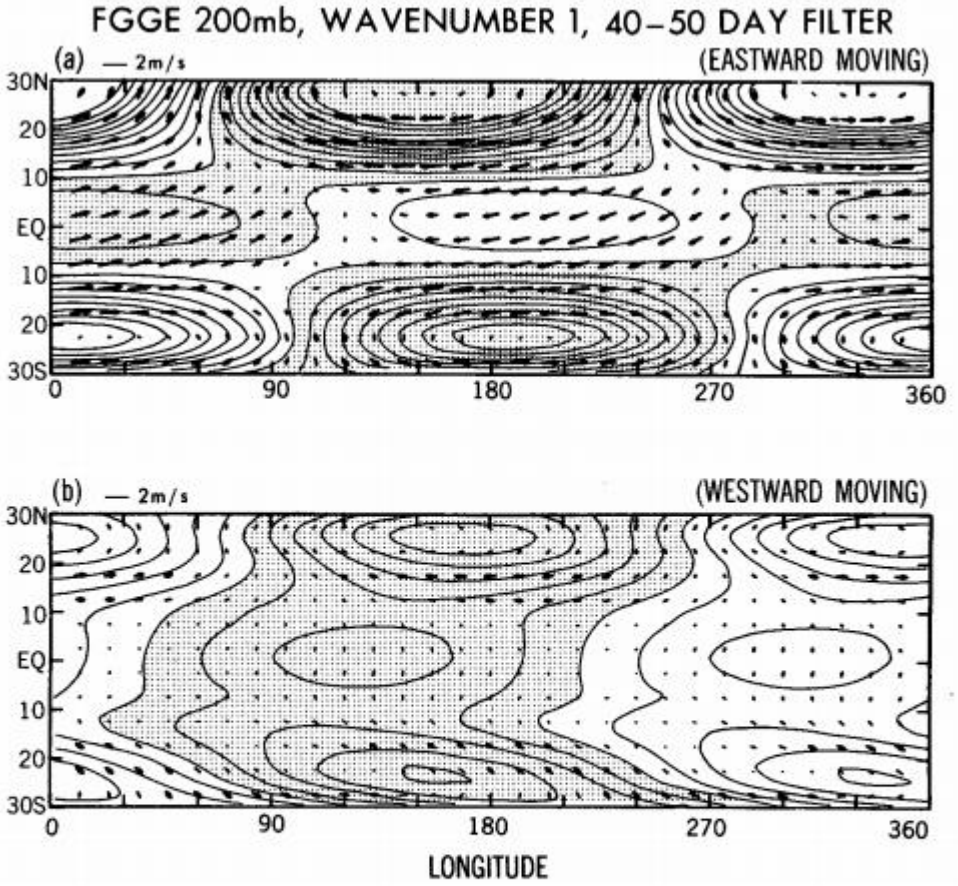

FIG. 6. Longitude–latitude sections (FGGE data, 200 mb) of the wavenumber-one, 40–50-day filtered wind vectors and geopotential height contours. The filtered data have been composited over one year along the longitude–time isoline of 10.3 m s^{-1} (a) eastward and (b) westward phase velocities. The contour interval is 1 m. Shading indicates positive values. The horizontal bar indicates the magnitude of the zonal component of the wind vectors. The latitudinal scale and the meridional component have been enlarged by a factor of 2 relative to the longitudinal scale and the zonal component, respectively.

5. Estrutura na escala planetária

a) Padrões de onda
   - Oscilações intrasazonais são associadas com 3 estruturas:
     - ✓ Planetária (propaga globalmente => nº de onda 1)
     - ✓ Supercluster (velocidade vertical concentrada propagando globalmente => nº de onda 5-10)
     - ✓ Regional (depende da localização; numerosos nº de onda

Apenas Rossby

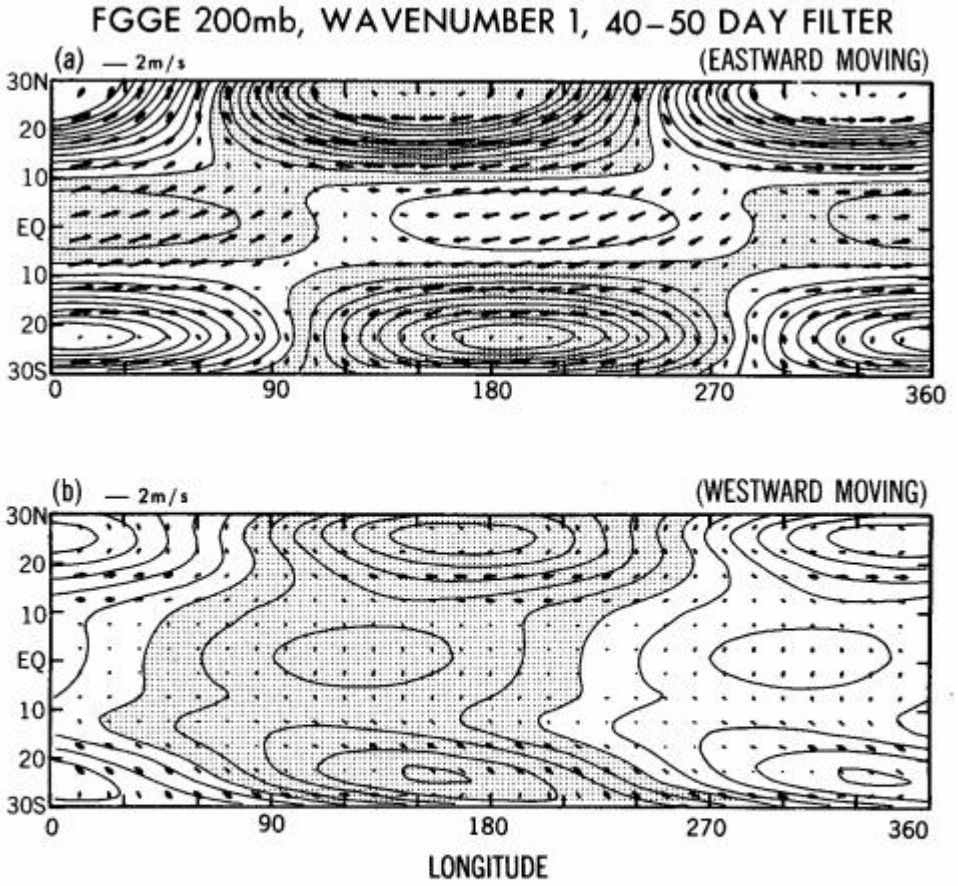

FIG. 6. Longitude–latitude sections (FGGE data, 200 mb) of the wavenumber-one, 40–50-day filtered wind vectors and geopotential height contours. The filtered data have been composited over one year along the longitude–time isoline of 10.3 m s^{-1} (a) eastward and (b) westward phase velocities. The contour interval is 1 m. Shading indicates positive values. The horizontal bar indicates the magnitude of the zonal component of the wind vectors. The latitudinal scale and the meridional component have been enlarged by a factor of 2 relative to the longitudinal scale and the zonal component, respectively.

Kelvin-Rossby

Geopotencial fora de fase com a vel. zonal perto do EQ (contrário Kelvin)

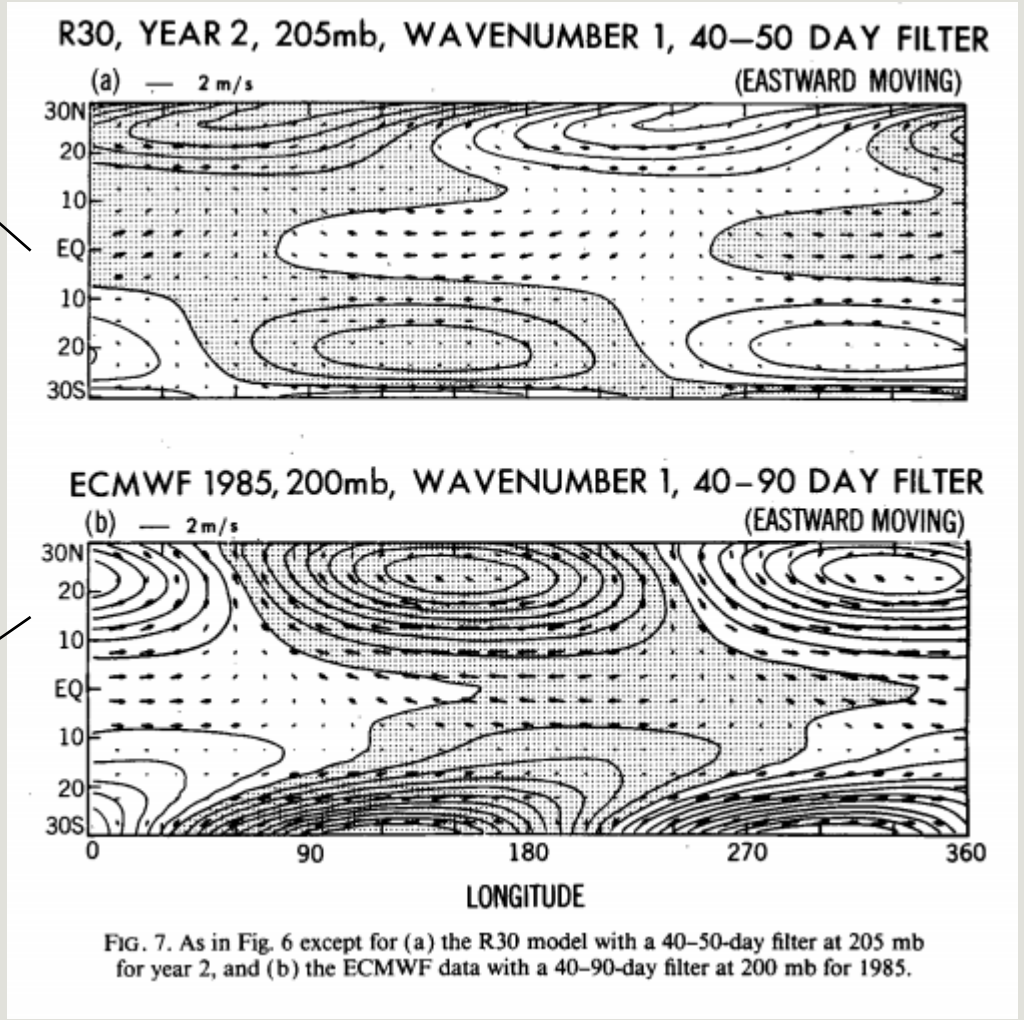

FIG. 7. As in Fig. 6 except for (a) the R30 model with a 40–50-day filter at 205 mb for year 2, and (b) the ECMWF data with a 40–90-day filter at 200 mb for 1985.

Sem padrão Kelvin
* causa: difusão vertical

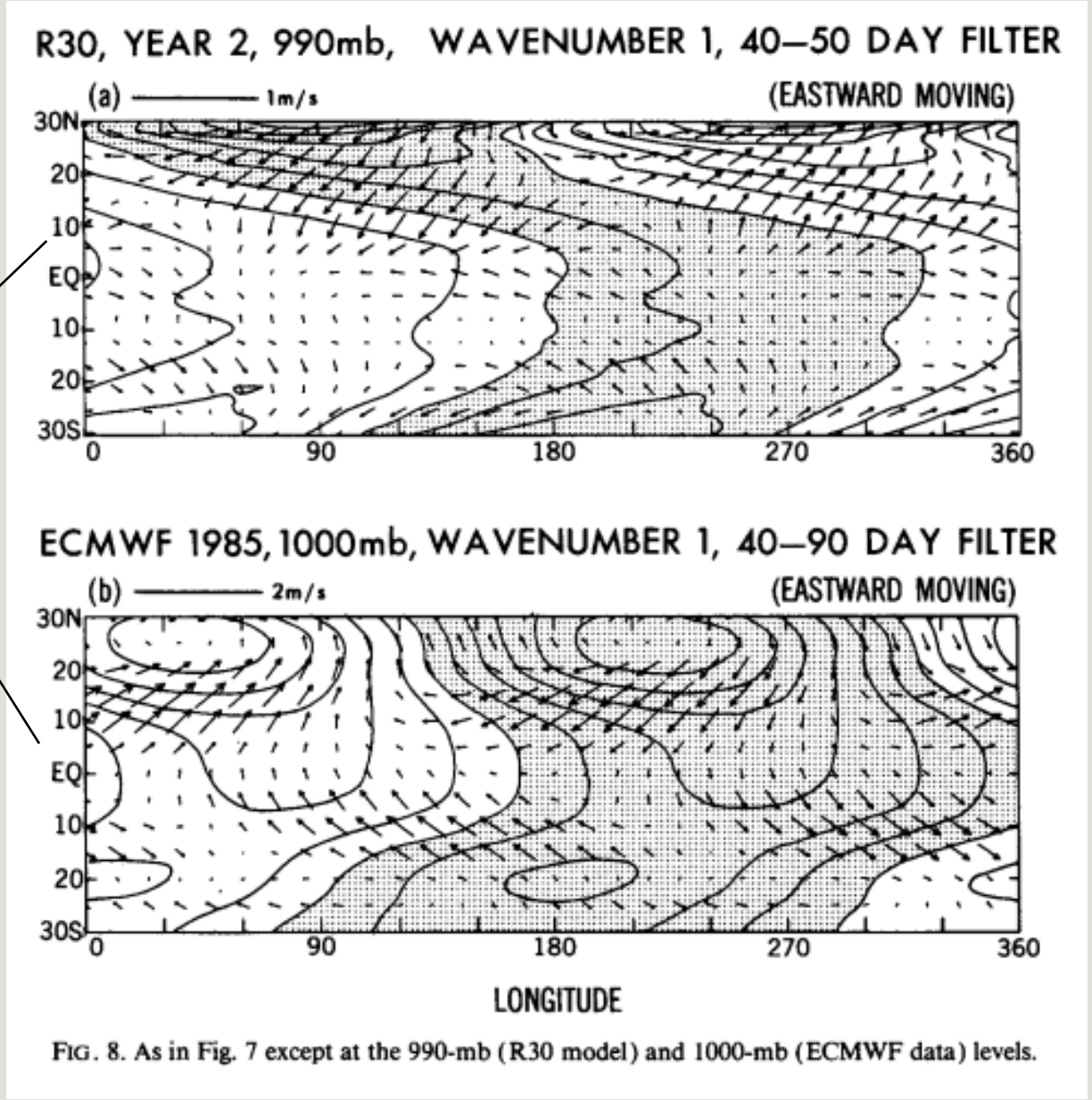

FIG. 8. As in Fig. 7 except at the 990-mb (R30 model) and 1000-mb (ECMWF data) levels.

b) Estrutura latitudinal

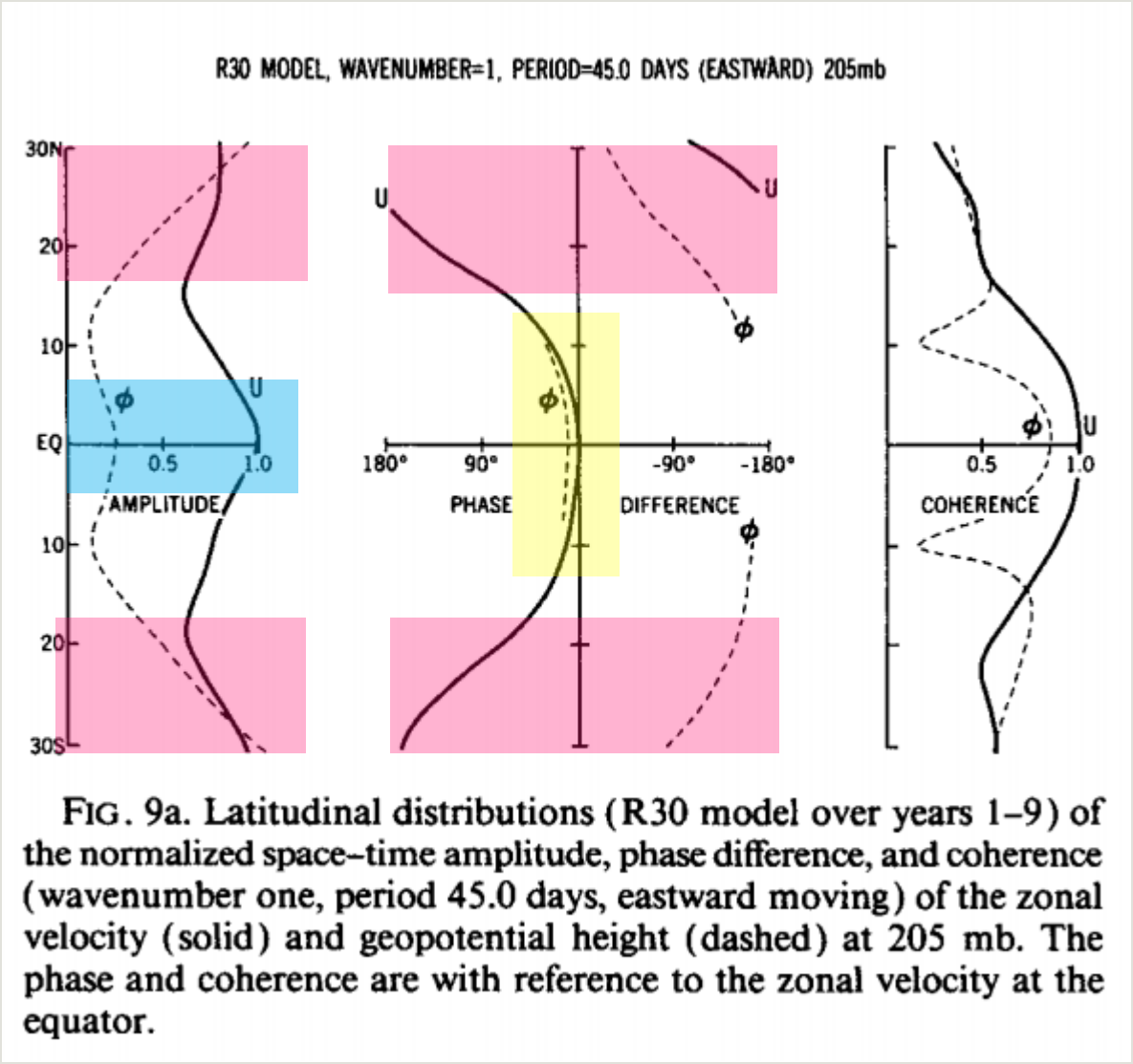

FIG. 9a. Latitudinal distributions (R30 model over years 1–9) of the normalized space–time amplitude, phase difference, and coherence (wavenumber one, period 45.0 days, eastward moving) of the zonal velocity (solid) and geopotential height (dashed) at 205 mb. The phase and coherence are with reference to the zonal velocity at the equator.

Máx local

Quase em fase

➡ Kelvin

Rossby

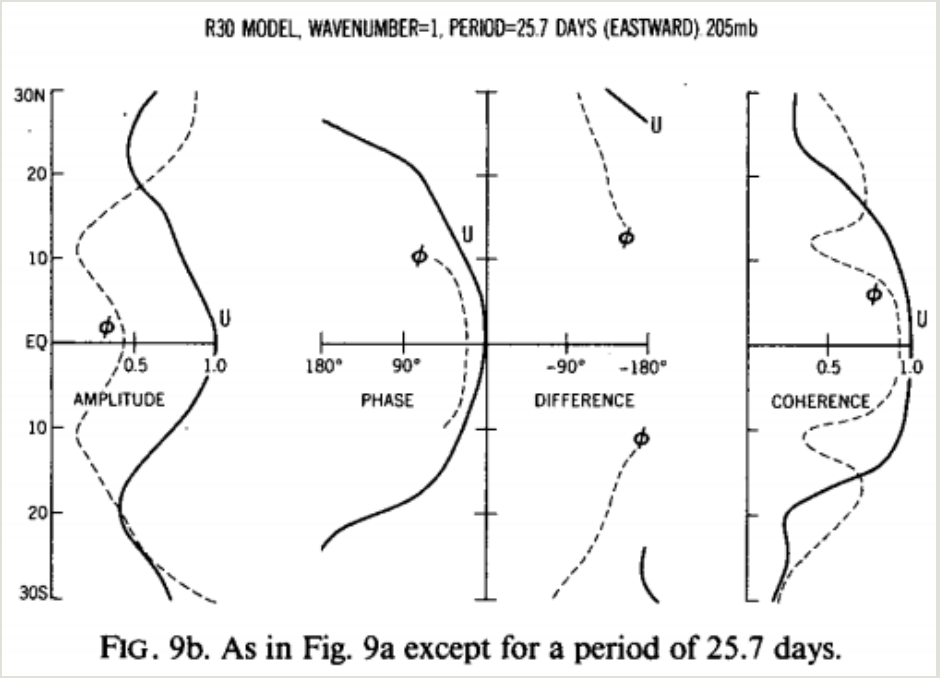

FIG. 9b. As in Fig. 9a except for a period of 25.7 days.

Sem máximo de u no EQ

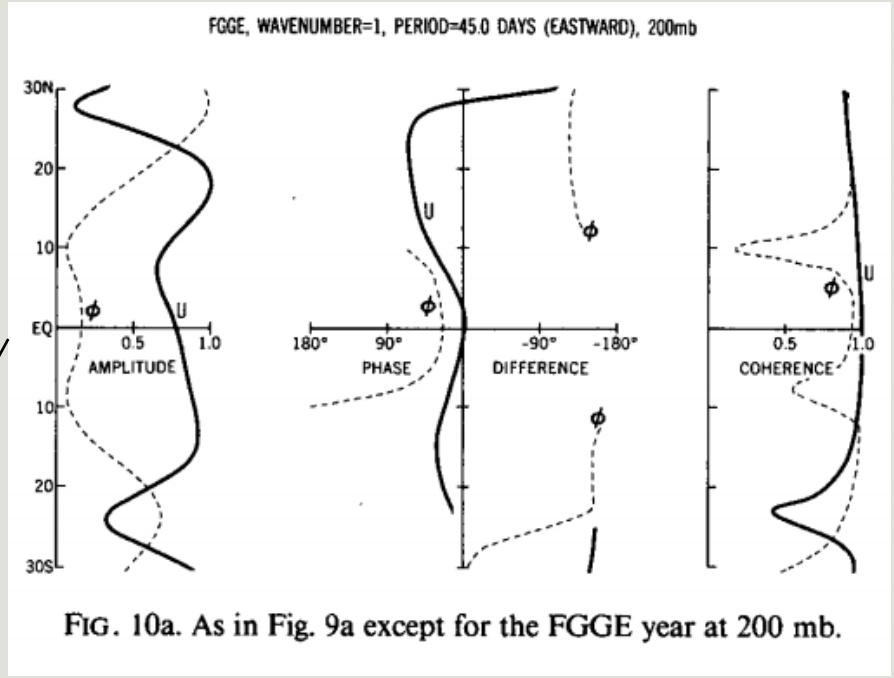

FIG. 10a. As in Fig. 9a except for the FGGE year at 200 mb.

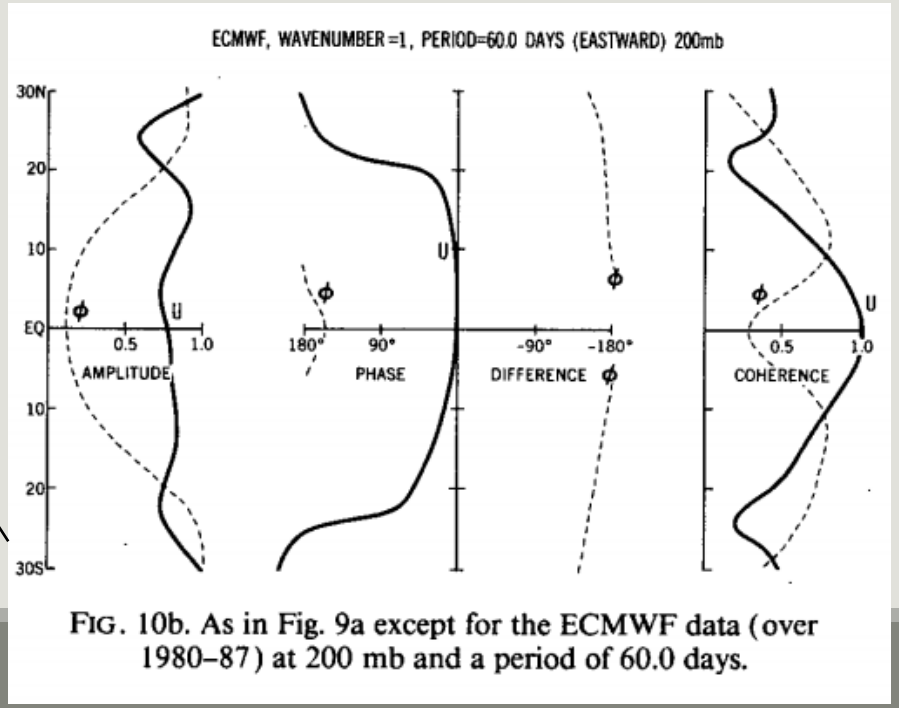

FIG. 10b. As in Fig. 9a except for the ECMWF data (over 1980–87) at 200 mb and a period of 60.0 days.

c) Estrutura vertical

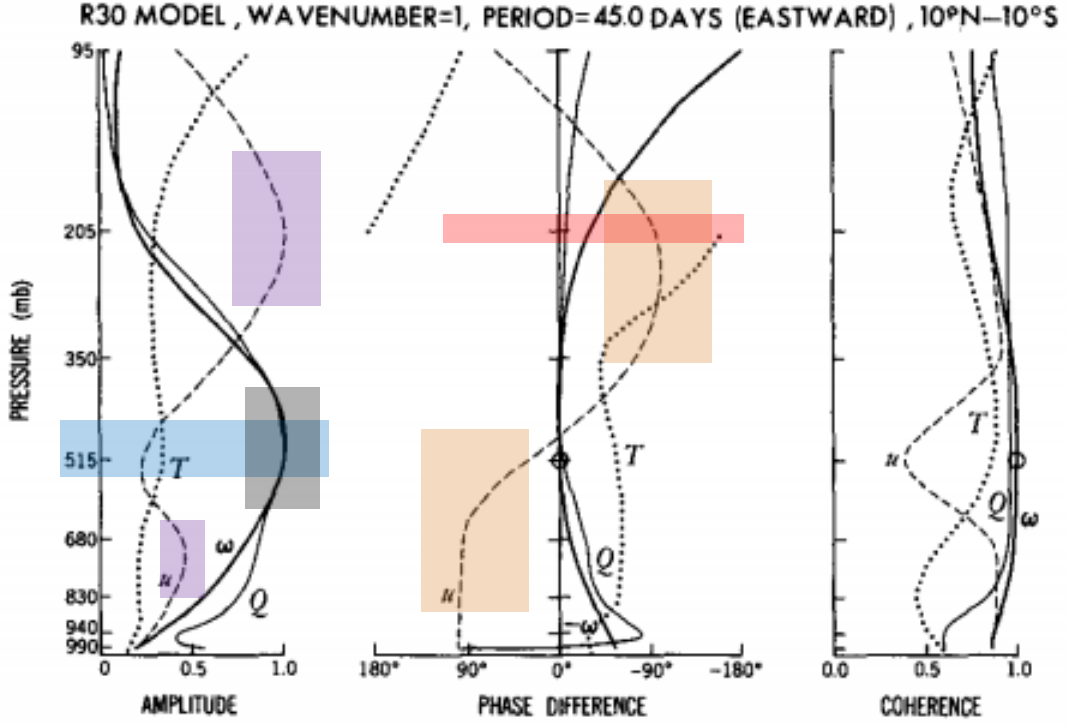

FIG. 11a. Vertical distributions (R30 model over years 1–9) of the normalized space–time amplitude, phase difference, and coherence (wavenumber one, period 45.0 days, eastward moving) of the zonal velocity (u, dashed), temperature (T, dotted), vertical pressure velocity ($-\omega$, thick solid), and convective heating (Q, thin solid) averaged between 10°N and 10°S. The phase and coherence are with reference to the 515-mb vertical pressure velocity, which is indicated by an open circle.

Máximos de u

Dif. de fase (~180°)

Máximo de ω

u e ω ~90° de defasagem

Máximo do aquecimento convectivo

Wave-CISK e resposta evaporação-vento

c) Estrutura vertical

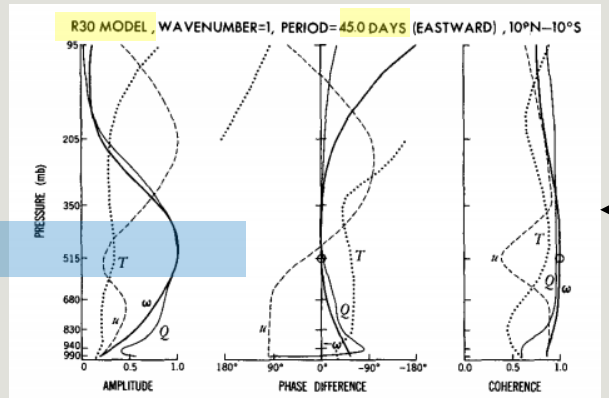

FIG. 11a. Vertical distributions (R30 model over years 1–9) of the normalized space–time amplitude, phase difference, and coherence (wavenumber one, period 45.0 days, eastward moving) of the zonal velocity (u, dashed), temperature (T, dotted), vertical pressure velocity ($-\omega$, thick solid), and convective heating (Q, thin solid) averaged between 10°N and 10°S. The phase and coherence are with reference to the 515-mb vertical pressure velocity, which is indicated by an open circle.

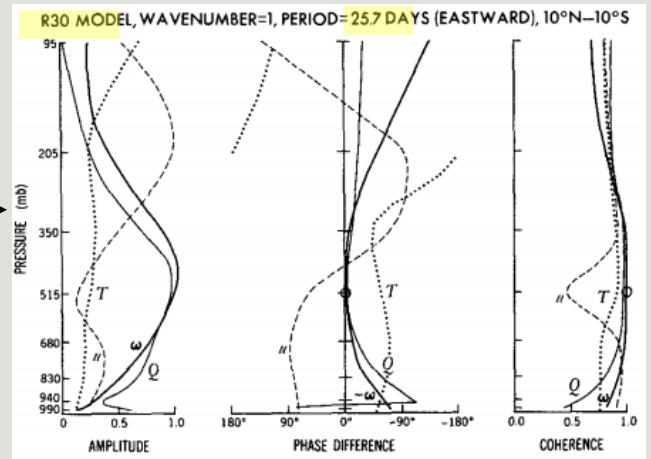

FIG. 11b. As in (a) except for the eastward-moving period of 25.7 days.

Máximo de ω acima de 300hPa

T e ω em fase

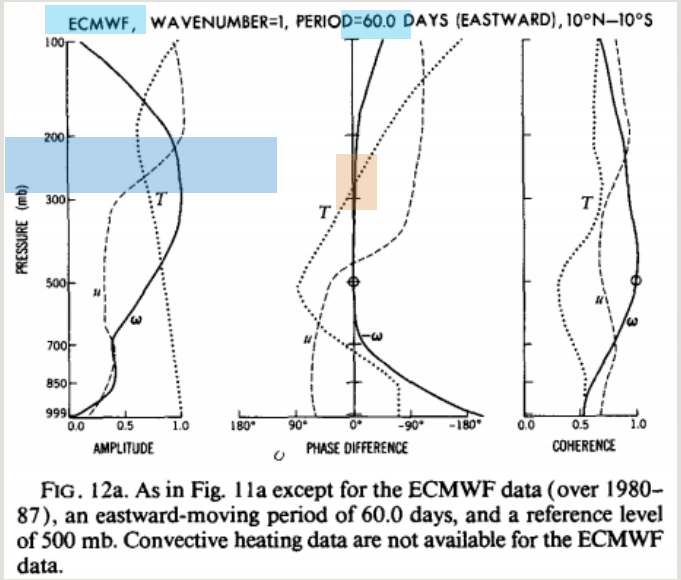

FIG. 12a. As in Fig. 11a except for the ECMWF data (over 1980–87), an eastward-moving period of 60.0 days, and a reference level of 500 mb. Convective heating data are not available for the ECMWF data.

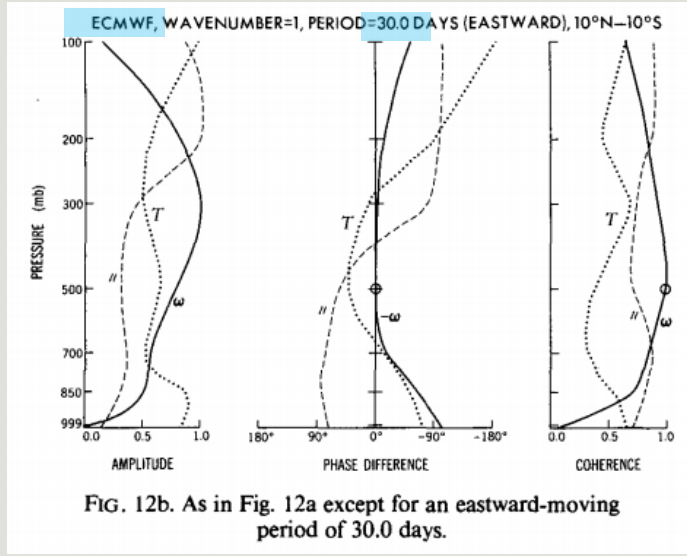

FIG. 12b. As in Fig. 12a except for an eastward-moving period of 30.0 days.

Similar ao modelo

6. Efeitos de uma maior resolução vertical

- Oscilações de 40-50 e 25-30 dias tem estruturas horizontais semelhantes mas algumas diferenças na estrutura vertical
- Análise no modelo SKYHI (resolução vertical de 1km)

6. Efeitos de uma maior resolução vertical

- Oscilações de 40-50 e 25-30 dias tem estruturas horizontais semelhantes mas algumas diferenças na estrutura vertical
- Análise no modelo SKYHI (resolução vertical de 1km)

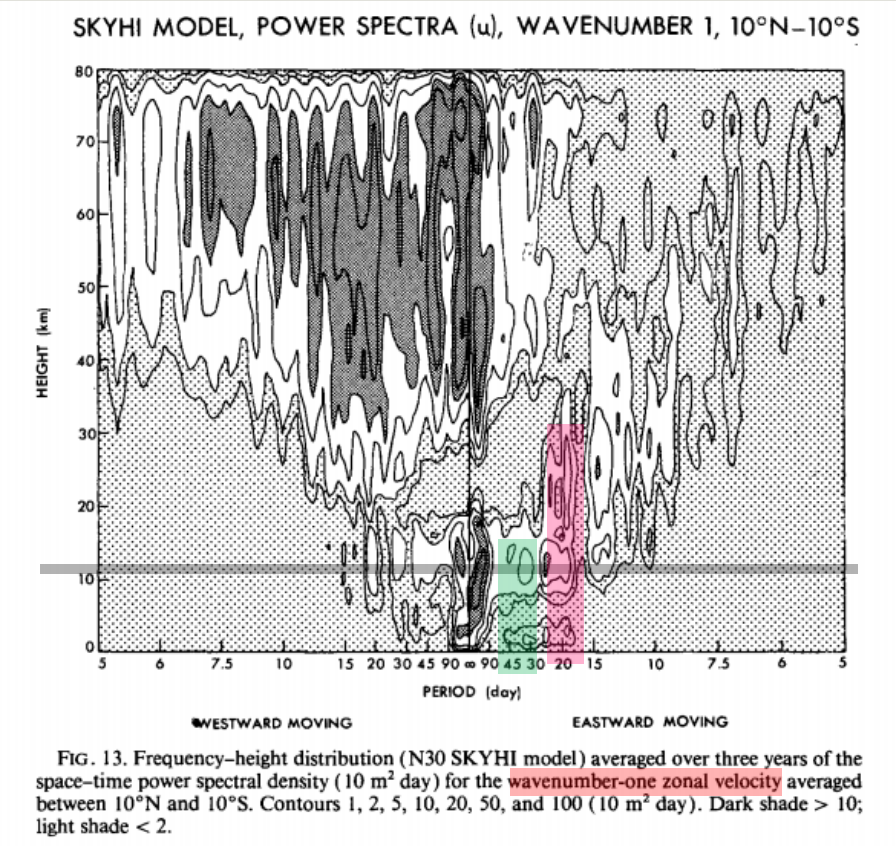

FIG. 13. Frequency–height distribution (N30 SKYHI model) averaged over three years of the space–time power spectral density ($10\ m^2$ day) for the wavenumber-one zonal velocity averaged between 10°N and 10°S. Contours 1, 2, 5, 10, 20, 50, and 100 ($10\ m^2$ day). Dark shade > 10; light shade < 2.

Pico confinado na troposfera

Chega na baixa estratosfera

6. Efeitos de uma maior resolução vertical

- Oscilações de 40-50 e 25-30 dias tem estruturas horizontais semelhantes mas algumas diferenças na estrutura vertical
- Análise no modelo SKYHI (resolução vertical de 1km)

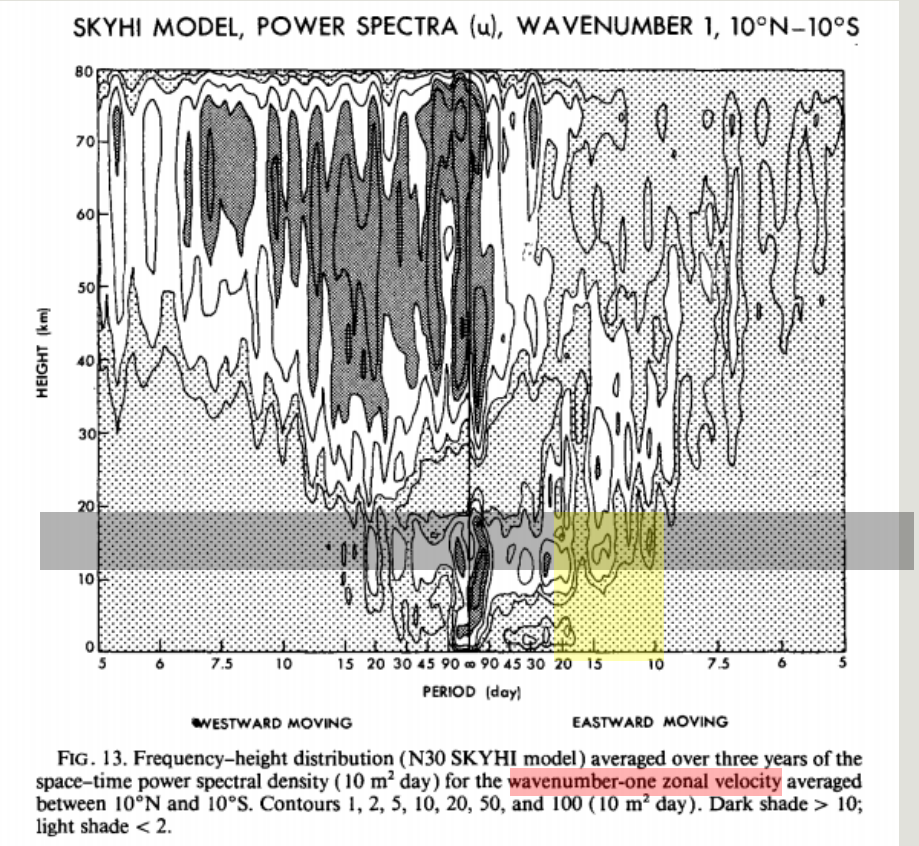

FIG. 13. Frequency–height distribution (N30 SKYHI model) averaged over three years of the space–time power spectral density ($10\ m^2$ day) for the wavenumber-one zonal velocity averaged between 10°N and 10°S. Contours 1, 2, 5, 10, 20, 50, and 100 ($10\ m^2$ day). Dark shade > 10; light shade < 2.

Onda de Kelvin estratosférica

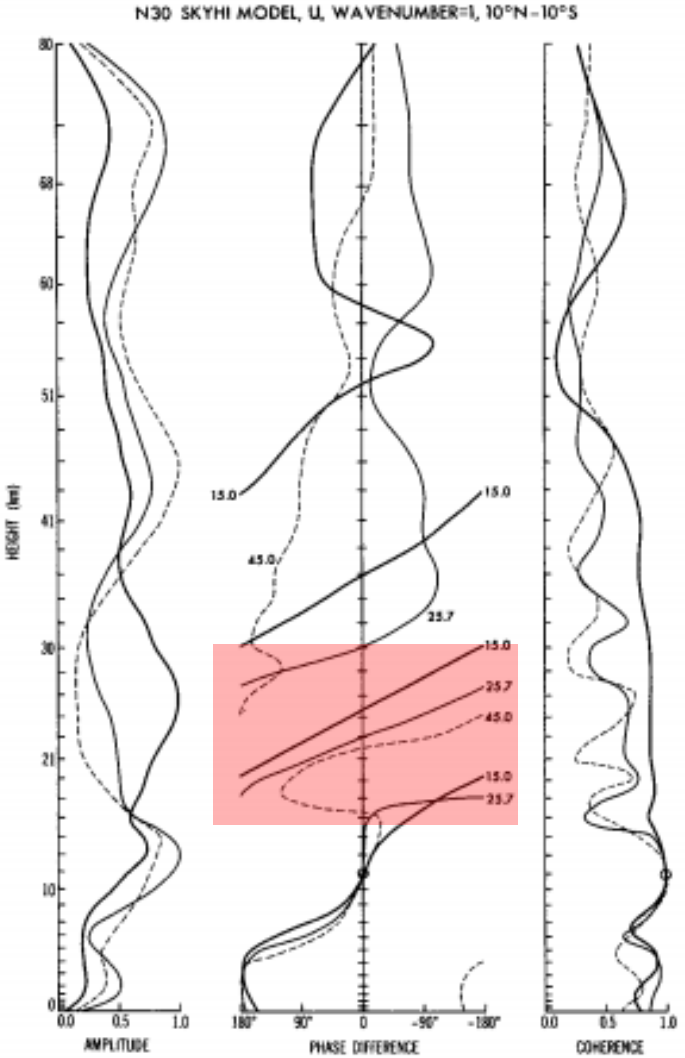

FIG. 14. Vertical distributions (N30 SKYHI model) averaged over three years of normalized space–time amplitude, phase difference, and coherence of the wavenumber-one zonal velocity averaged between 10°N and 10°S. The curves are drawn for eastward-moving periods of 45.0 (dashed), 25.7 (thin solid), and 15.0 (thick solid) days. The phase and coherence distributions are with reference to the 102-mb level. The tick marks indicate the vertical resolution of the model.

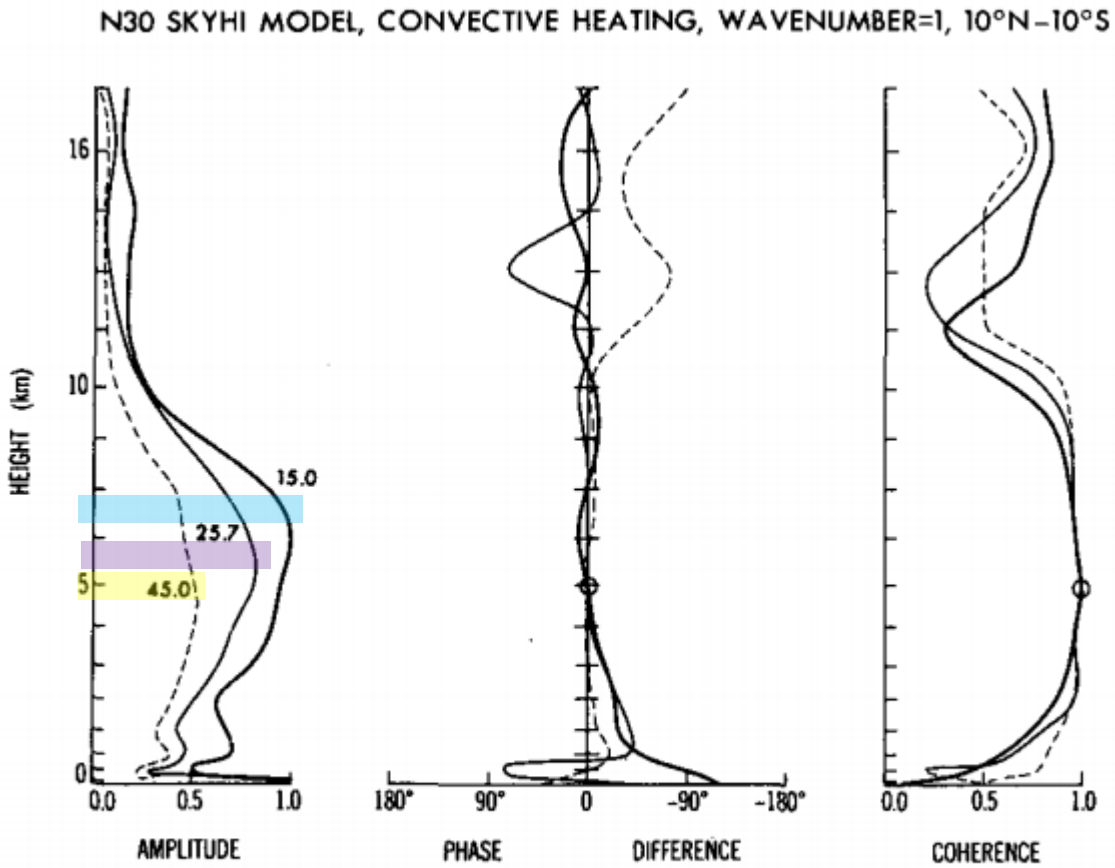

FIG. 15. As in Fig. 14 except for tropospheric convective heating at heights between 0 and 17 km.

- Diferença de fase na baixa e alta troposfera
- Diferença no nº de onda vertical intrínseco (não aparece no modelo R30 de nove níveis)

7. Efeitos de variações geográficas e sazonais

a) Oscilações na escala planetária
   - Os picos espectrais de 40-50 e 25-30 dias não resultam das mudanças advectivas das velocidades de fase intrínsecas por diferentes fluxos básicos locais; nem da modulação não-linear de seus períodos intrínsecos por ciclos sazonais
   - Demonstração: essas oscilações apareceriam num modelo de superfície oceânica sem variação sazonal
   - Efeitos da TSM na distribuição geográfica da precipitação
   - Isolar oscilações não lineares localizadas de escala *supercluster* das oscilações de escala planetária geograficamente localizadas

7. Efeitos de variações geográficas e sazonais

a) Oscilações na escala planetária

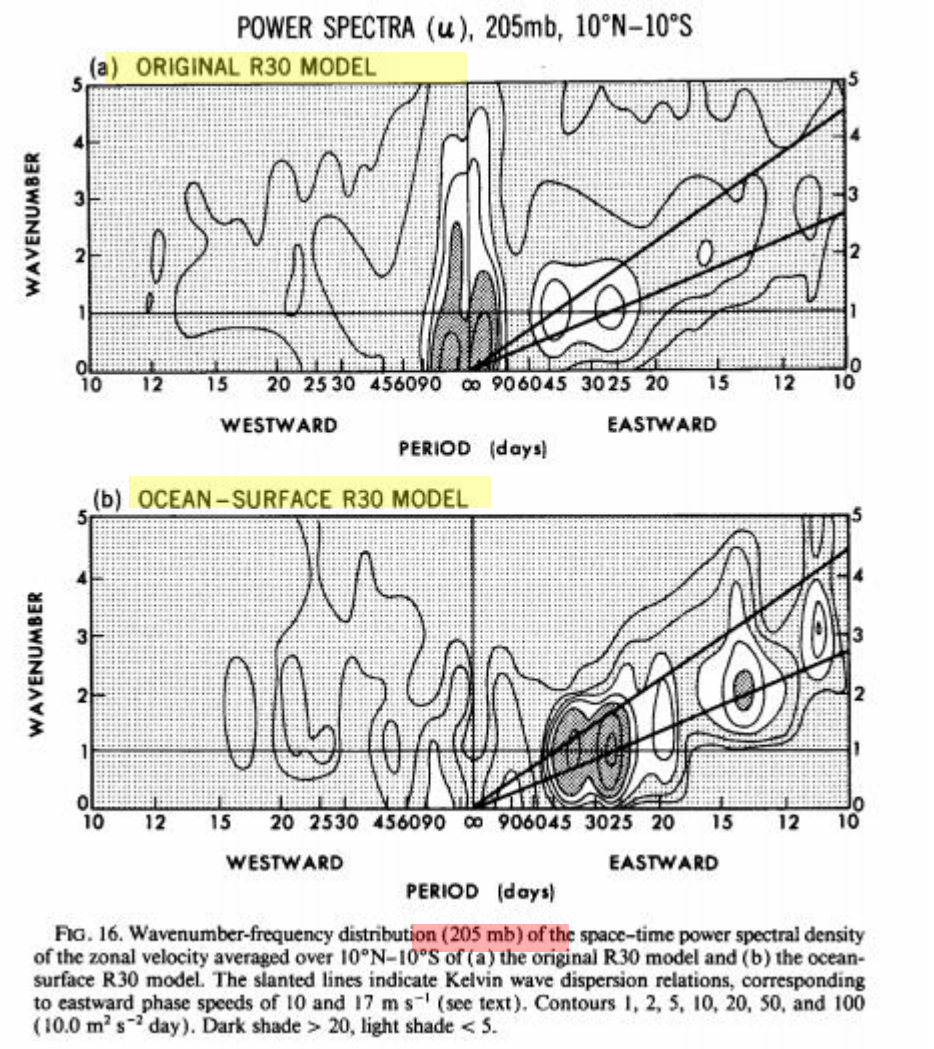

FIG. 16. Wavenumber-frequency distribution (205 mb) of the space–time power spectral density of the zonal velocity averaged over 10°N–10°S of (a) the original R30 model and (b) the ocean-surface R30 model. The slanted lines indicate Kelvin wave dispersion relations, corresponding to eastward phase speeds of 10 and 17 m s^{-1} (see text). Contours 1, 2, 5, 10, 20, 50, and 100 (10.0 m^2 s^{-2} day). Dark shade > 20, light shade < 5.

7. Efeitos de variações geográficas e sazonais

a) Oscilações na escala planetária

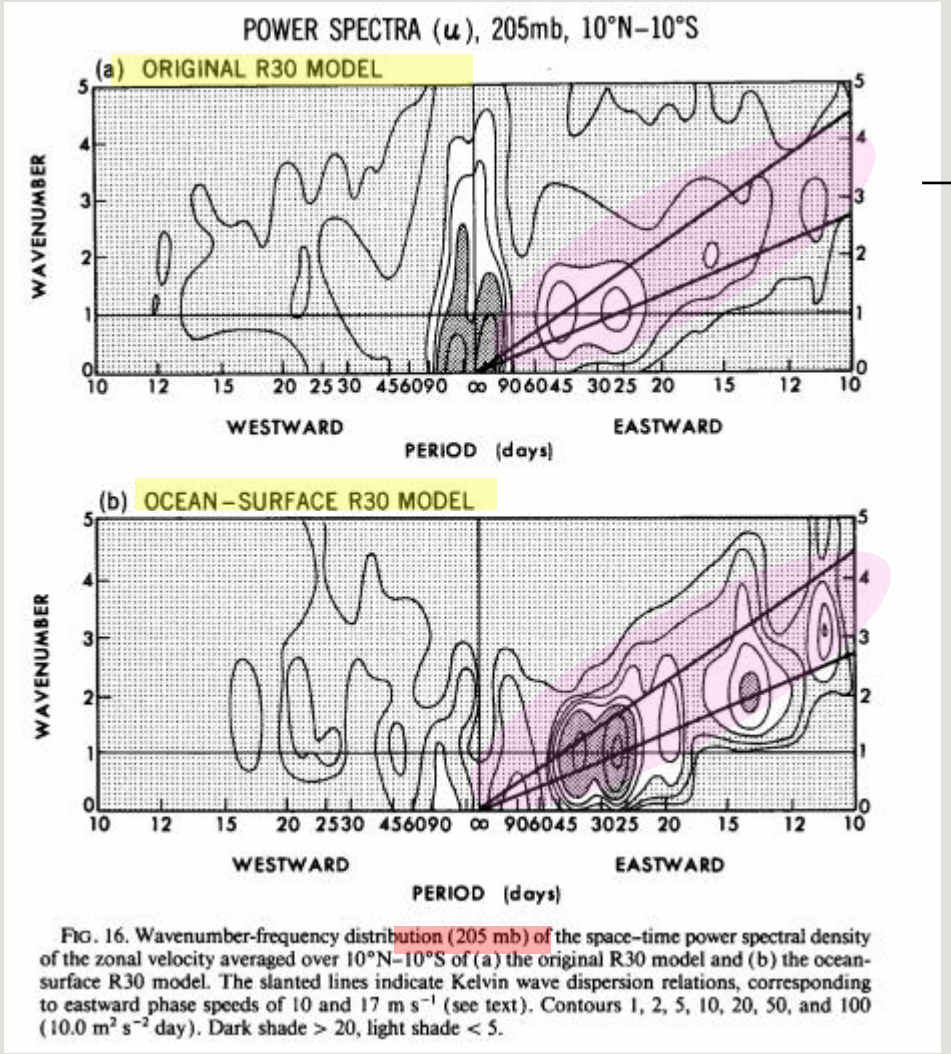

FIG. 16. Wavenumber-frequency distribution (205 mb) of the space–time power spectral density of the zonal velocity averaged over 10°N–10°S of (a) the original R30 model and (b) the ocean-surface R30 model. The slanted lines indicate Kelvin wave dispersion relations, corresponding to eastward phase speeds of 10 and 17 m s^{-1} (see text). Contours 1, 2, 5, 10, 20, 50, and 100 (10.0 m^2 s^{-2} day). Dark shade > 20, light shade < 5.

Magnitude comparável com fig1

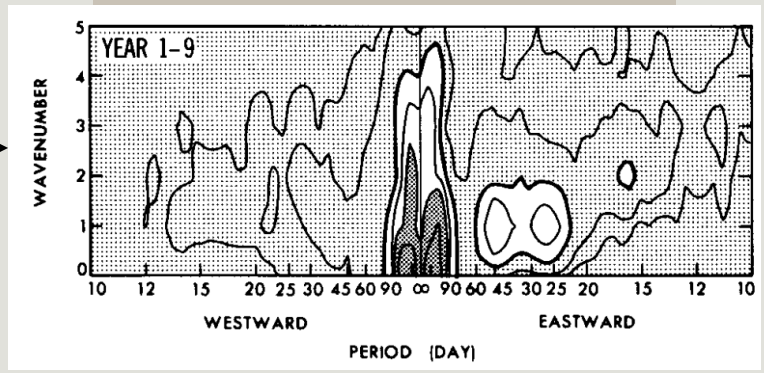

Magnitudes diferentes para as oscilações de 40-50 e 25-30 dias; picos mais fortes (prec. não localizada geograficamente)

Linhas de dispersão das ondas de Kelvin

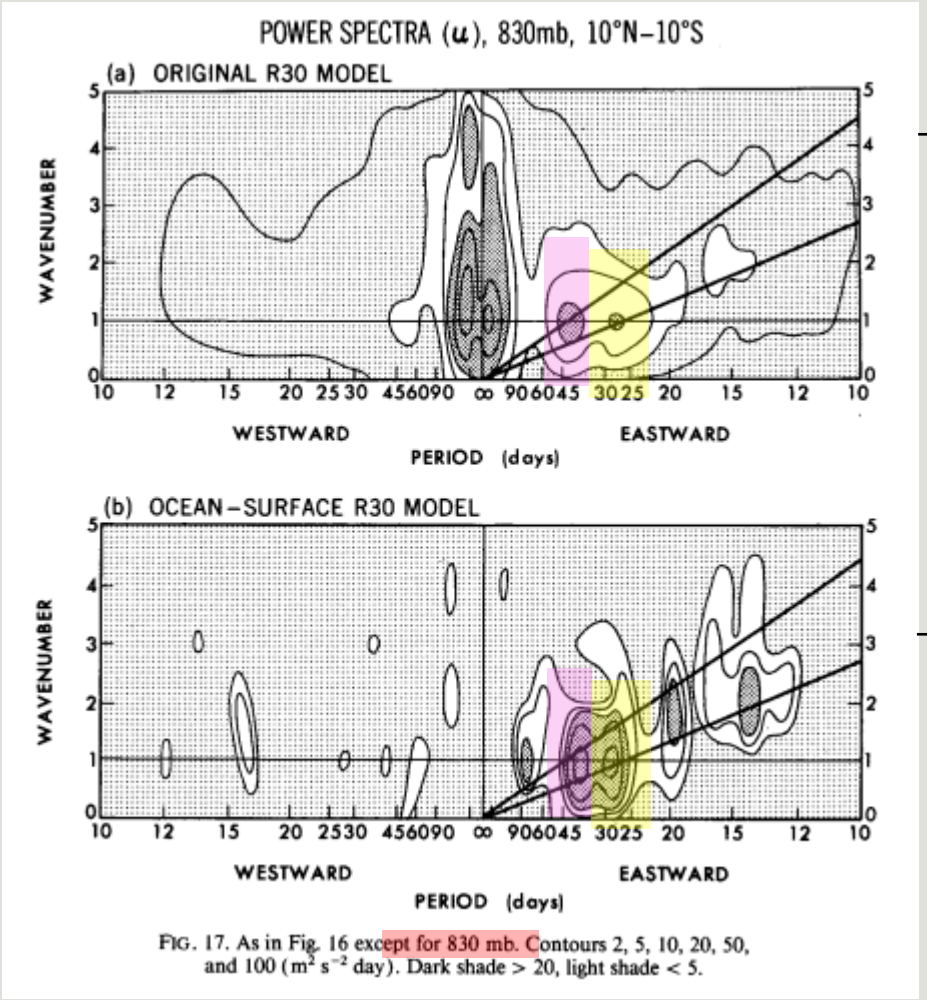

FIG. 17. As in Fig. 16 except for 830 mb. Contours 2, 5, 10, 20, 50, and 100 ($m^2 s^{-2}$ day). Dark shade > 20, light shade < 5.

40-50 mais forte que 25-30

Comparáveis; mais fortes que o modelo original

Dif. entre 205hPa e 830hPa: diferentes distribuições verticais das amplitudes das velocidades zonais

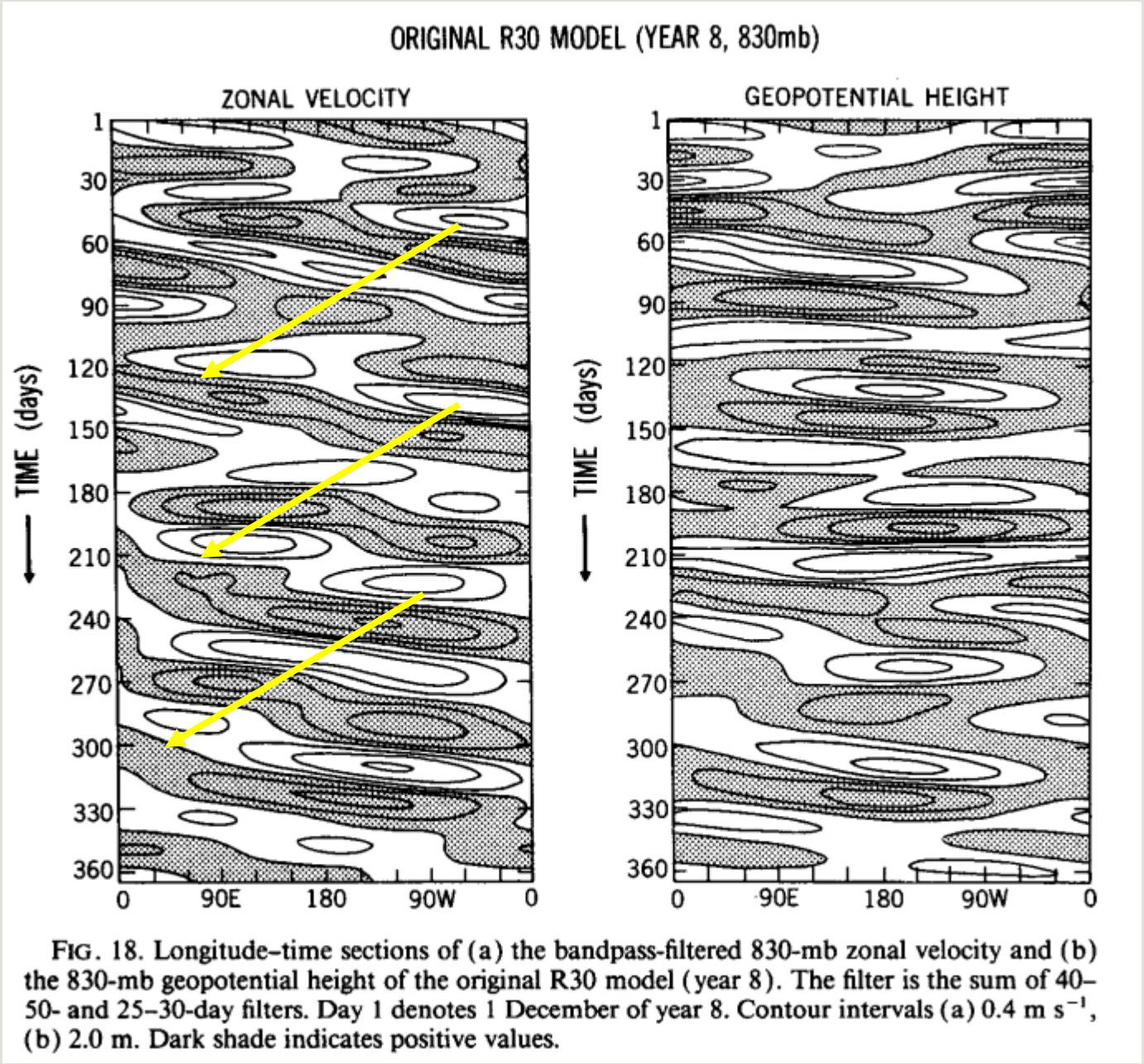

FIG. 18. Longitude–time sections of (a) the bandpass-filtered 830-mb zonal velocity and (b) the 830-mb geopotential height of the original R30 model (year 8). The filter is the sum of 40–50- and 25–30-day filters. Day 1 denotes 1 December of year 8. Contour intervals (a) 0.4 m s^{-1}, (b) 2.0 m. Dark shade indicates positive values.

- Soma das oscilações 40-50 e 25-30 dias e seu deslocamento no tempo
- A velocidade zonal é uma onda movendo-se para leste
- A altura geopotencial é estacionária

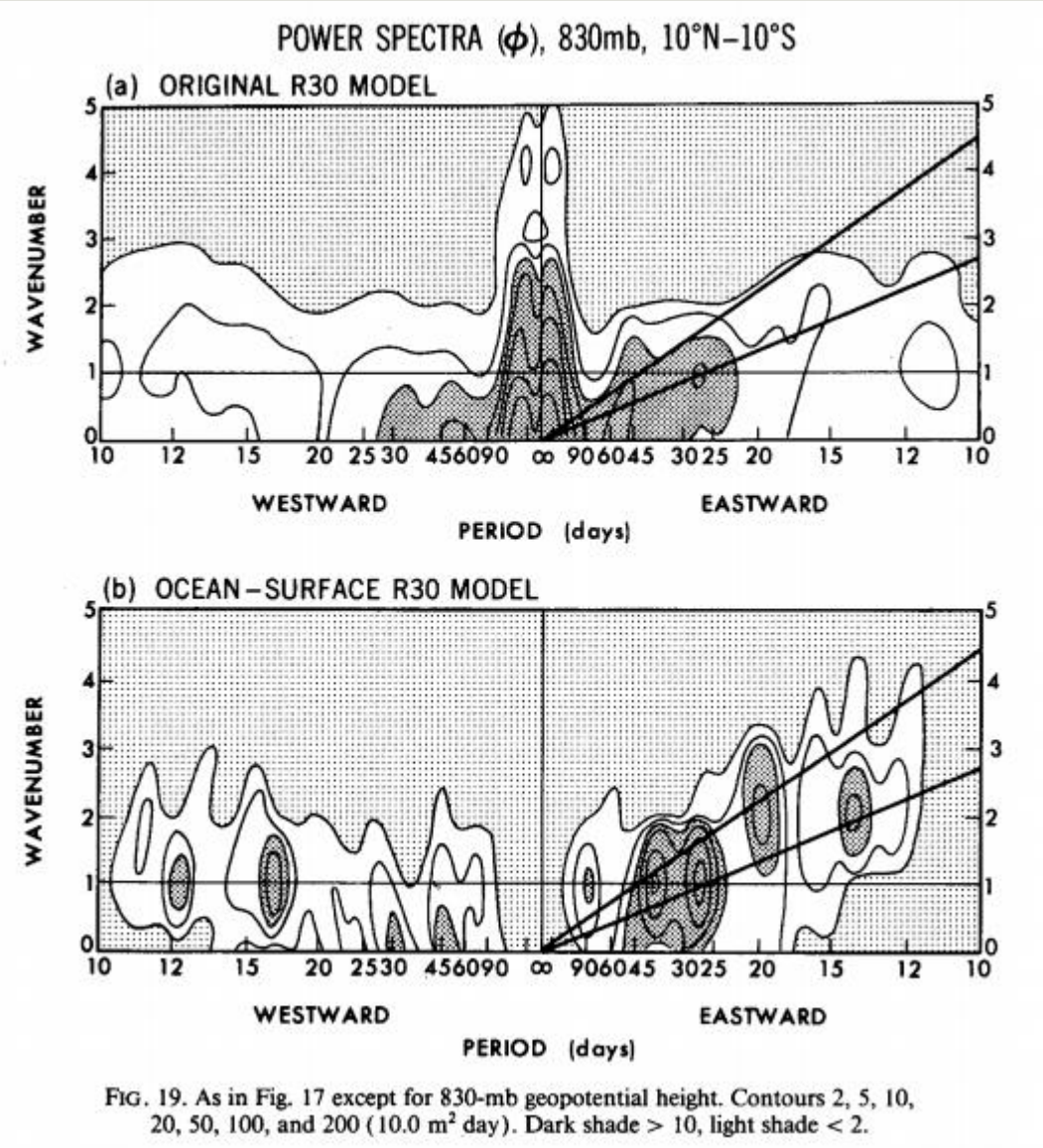

FIG. 19. As in Fig. 17 except for 830-mb geopotential height. Contours 2, 5, 10, 20, 50, 100, and 200 (10.0 m^2 day). Dark shade > 10, light shade < 2.

Estacionário:
R30 original => nº onda 1 e 0 (média zonal), para leste e oeste, mesma magnitude

As duas oscilações são simuladas para um modelo com superfície oceânica

b) Oscilações na escala supercluster (nº onda 5-10)

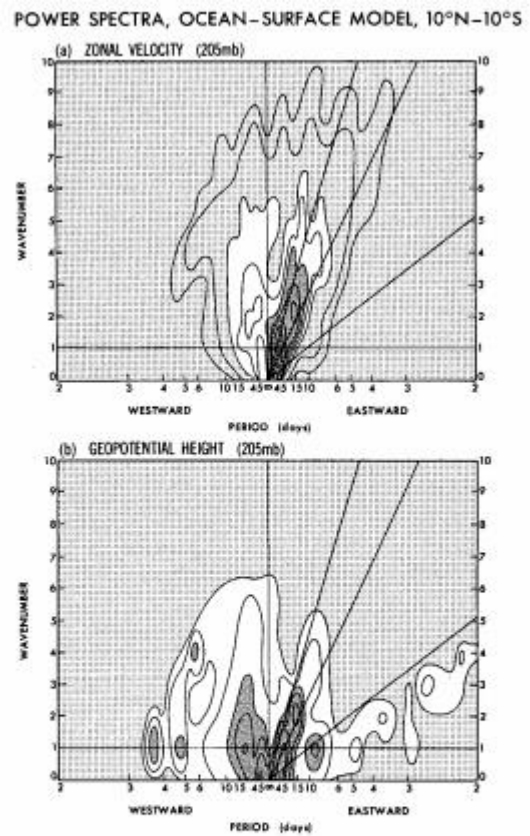

FIG. 20. Wavenumber-frequency distribution (ocean surface R30 model) of the space–time spectral density of the (a) 205-mb zonal velocity and (b) geopotential height averaged between 10°N and 10°S for the range of wavenumbers 0–10 and periods from 2 days westward to 2 days eastward. Slanted lines indicate Kelvin wave dispersion relations corresponding to eastward phase velocities of 10, 17, and 45 m s^{-1} (see text). Contours (a) 5, 10, 20, 50, 100, 200, and 500 (m^2 s^{-2} day); Dark shade > 20, light shade < 5. Contours (b) 1, 2, 5, 10, 20, 50, and 100 (10.0 m^2 day); Dark shade > 10, light shade < 2.

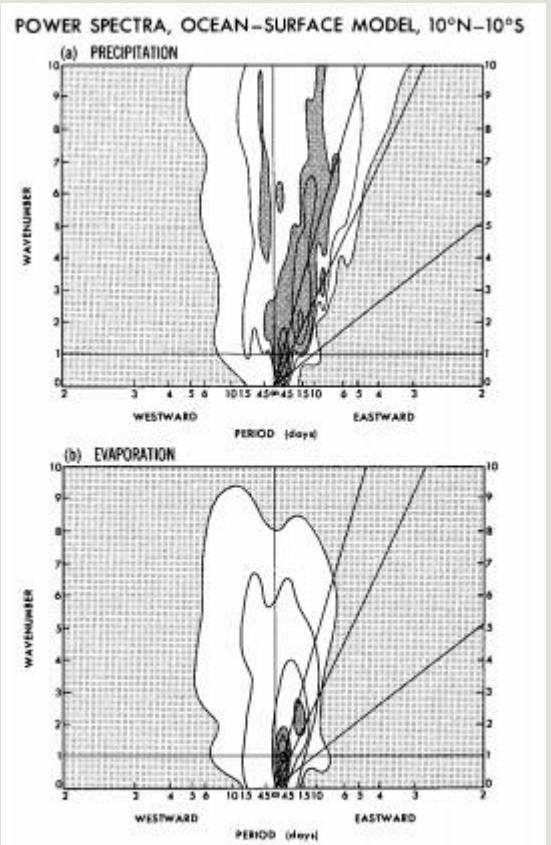

FIG. 21. As in Fig. 20 except for (a) precipitational heating and (b) evaporational cooling. Contours (a) 2, 5, 10, 20, and 50 (234.0 W2 m^{-4} day); Dark shade > 10, light shade < 2. Contours (b) 1, 2, 5, 10, 20, and 50 (23.4 W2 m^{-4} day); Dark shade > 10, light shade < 1.

Sem distinção das oscilações

c) Relação entre a precipitação e a velocidade vertical

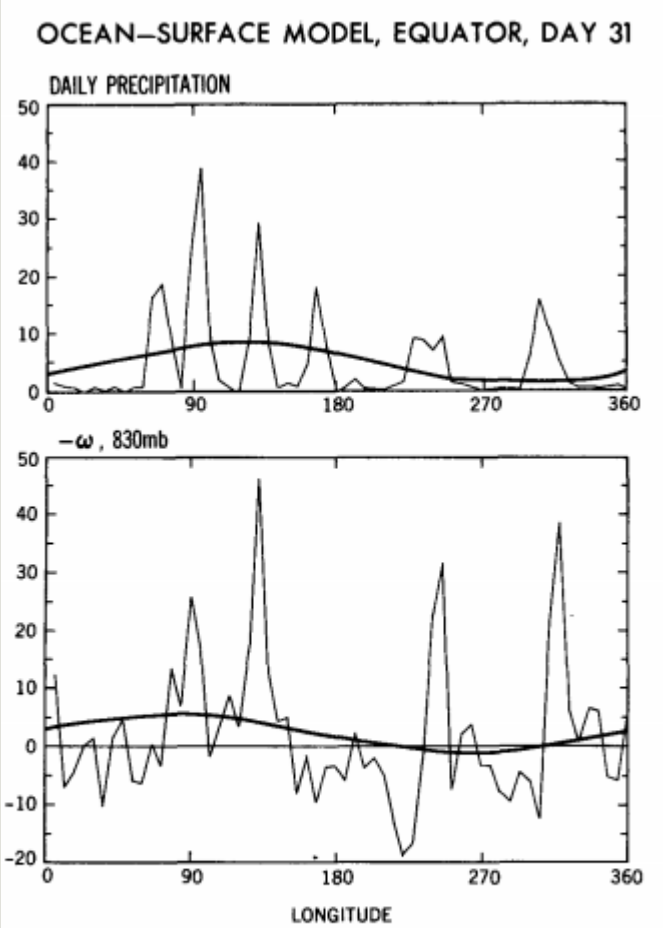

FIG. 22. Longitude distribution of (a) daily precipitational heating and (b) 830-mb vertical pressure velocity of the ocean surface R30 model (day 31, year 2) at the equator. Thin and thick lines indicate wavenumber 0–30 and 0–1 components, respectively. The units are (a) 48.4 W m^{-2} and (b) 10^{-10} Pa s^{-1}.

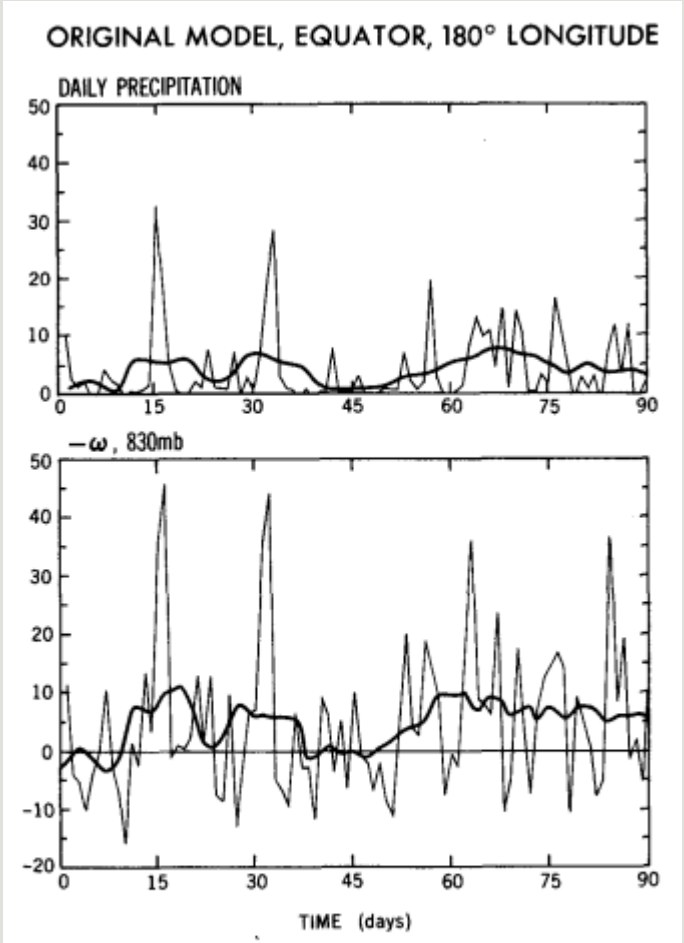

FIG. 23. Time distribution over 90 days of daily precipitational heating (a) and 830-mb vertical pressure velocity of the original R30 model (year 8) at 180° longitude. Day 1 denotes 1 December. Thin and thick lines indicate daily and 11-day running mean values, respectively. The units are (a) 48.4 W m^{-2} and (b) 10^{-10} Pa s^{-1}.

Precipitação ⇔ movimento vertical ascendente

Umidade ⇔ convergência de vapor d'água e evaporação

d) Propagação das oscilações da escala planetária e supercluster

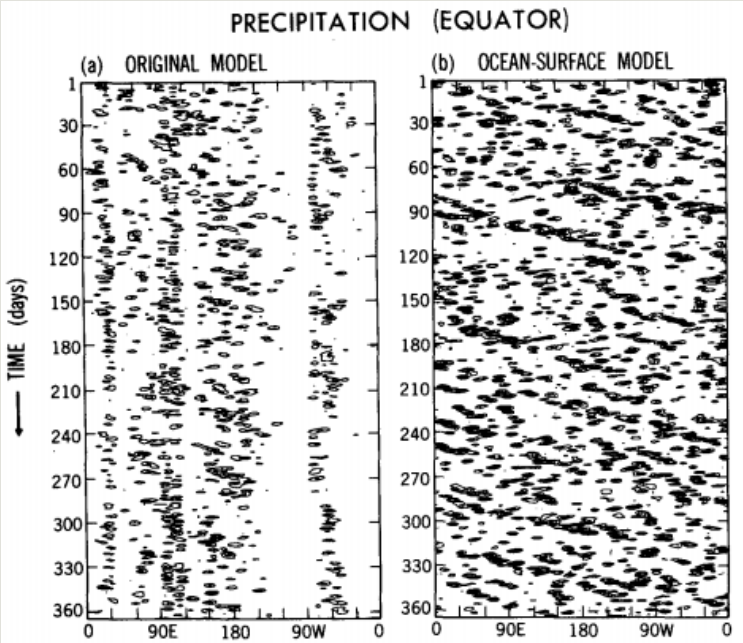

FIG. 24. Longitude–time distribution of daily precipitational heating at the equator of (a) the original R30 model and (b) the ocean surface R30 model. The seasonal variation has been subtracted from the original model precipitation. Day 1 denotes (a) 1 December of year 8 and (b) the first day of year 2. Contours are drawn for positive values only. Contour values are (a) 5, 20, 35, 50, and 65 (48.4 W m^{-2}) and (b) 6, 12, 18, 24, 30, 36, 42, 48, 54, 60, and 66 (48.4 W m^{-2}).

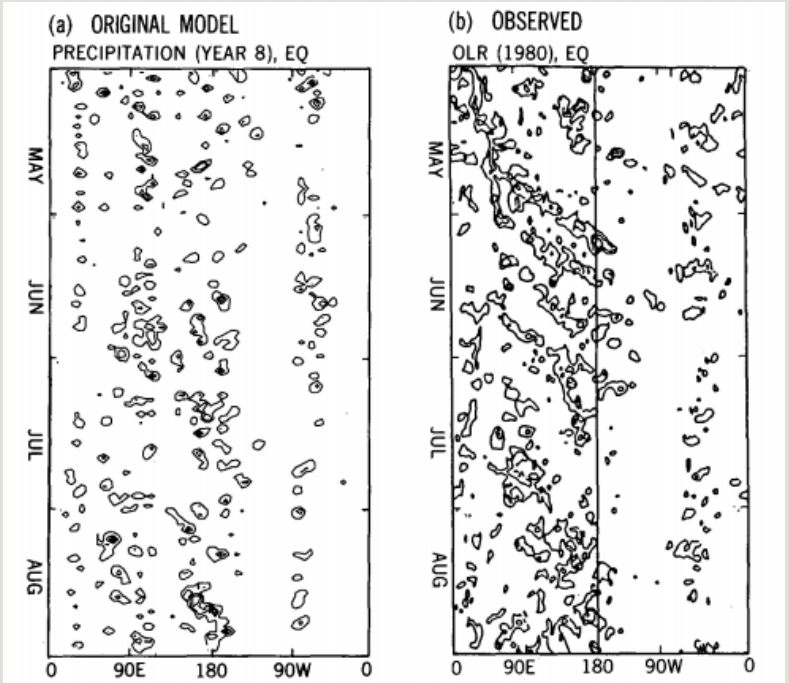

FIG. 25. Longitude–time distribution (May–August, equator) of (a) the daily precipitational heating of the original R30 model and (b) the observed outgoing longwave radiation for the year 1980 (after Hayashi and Nakazawa 1989). The seasonal variation was subtracted. Contours are drawn for (a) positive and (b) negative values only. Contour values are (a) 5, 20, 35, 50, and 65 (48.4 W m^{-2}) and (b) −20, −60, and −100 (W m^{-2}).

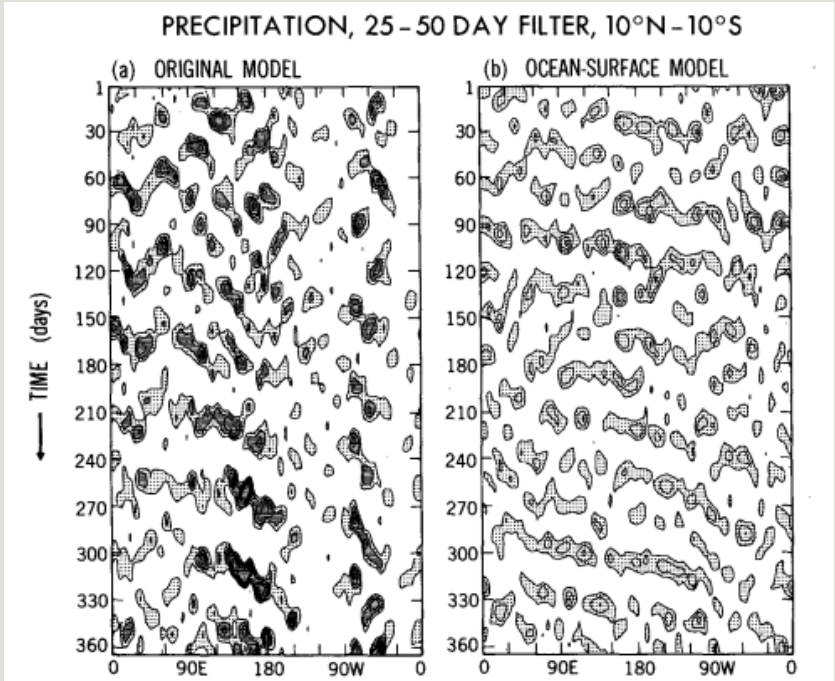

FIG. 26. As in Fig. 24 except for the sum of 40–50- and 25–30-day filtered precipitational heating averaged over 10°N–10°S. Contours are drawn for positive values only. Contour values are (a) 2, 6, 10, 14, and 18 (4.84 W m^{-2}) and (b) 3, 9, 15, and 21 (4.84 W m^{-2}).

Modelo original: concentração da chuva em determinadas longitudes; leve propagação para leste (mais evidente no modelo com o oceano)

8. Conclusões e observações

- Nº de onda 1, mov. para leste: dois picos de magnitudes comparáveis (40-50 e 25-30 dias)
- Distribuição horizontal da variância similar
- Kelvin: movimento para leste na alta troposfera
- Rossby: movimento para leste fora do Equador
- Oscilações tem estrutura horizontal e vertical parecidas; ocorrem mesmo sem variações geográficas locais ou sazonais
- TSM modula a propagação da precipitação
- Modelo ⇔ dados observados

Referências

where the phase speed c is given by

$$c = -\frac{\sigma}{k}. \qquad \text{(A9)}$$

In the presence of a basic flow U, the phase speed and frequency are replaced by the relative phase speed $(c - U)$ and intrinsic frequency $(\sigma + kU)$, respectively.

REFERENCES

Anderson, J. R., and R. D. Rosen, 1983: The latitude–height structure of 40–50-day variations in atmospheric angular momentum. *J. Atmos. Sci.*, **40**, 1584–1591.

——, and D. E. Stevens, 1987: The presence of linear wavelike modes in a zonally symmetric model of the tropical atmosphere. *J. Atmos. Sci.*, **44**, 2115–2127.

Arakawa, A., and W. H. Schubert, 1974: Interaction of a cumulus cloud ensemble with the large-scale environment. Part I. *J. Atmos. Sci.*, **31**, 674–701.

Bengtsson, L., M. Kanamitsu, P. Kallberg, and S. Uppals, 1982: FGGE four-dimensional data assimilation at ECMWF. *Bull. Amer. Meteor. Soc.*, **63**, 29–43.

Chang, C.-P., 1976: Forcing of stratospheric Kelvin waves by tropospheric heat sources. *J. Atmos. Sci.*, **33**, 740–744.

——, 1977: Viscous internal gravity waves and low-frequency oscillations in the tropics. *J. Atmos. Sci.*, **34**, 901–910.

——, and H. Lim, 1988: Kelvin wave–CISK: A possible mechanism for the 30–50-day oscillations? *J. Atmos. Sci.*, **45**, 1709–1720.

Chao, W. C., 1987: On the origin of the tropical intraseasonal oscillation. *J. Atmos. Sci.*, **44**, 1940–1949.

Chen, T.-C., 1985: On the time variation in the tropical energetics of large-scale motions during the FGGE summer. *Tellus*, **37A**, 258–275.

Crum, F. X., and T. J. Dunkerton, 1992: Analytic and numerical models of wave-CISK with conditional heating. *J. Atmos. Sci.*, **49**, 1693–1708.

Davey, M. K., 1989: A simple tropical moist model applied to the "40-day" wave. *Quart. J. Roy. Meteor. Soc.*, **115**, 1071–1107.

Davis, H. C., 1979: Phase-lagged wave–CISK. *Quart. J. Roy. Meteor. Soc.*, **105**, 323–353.

Dunkerton, T. J., and F. X. Crum, 1991: Scale-selection and propagation of wave–CISK with conditional heating. *J. Meteor. Soc. Japan*, **69**, 449–458.

Emanuel, K. A., 1987: An air–sea interaction model of intraseasonal oscillations in the tropics. *J. Atmos. Sci.*, **44**, 2324–2340.

Garcia, R. R., and M. L. Salby, 1987: Transient response to localized episodic heating in the tropics. Part II: Far-field behavior. *J. Atmos. Sci.*, **44**, 499–530.

Gill, A. E., 1980: Some simple solutions for heat-induced tropical circulation. *Quart. J. Roy. Meteor. Soc.*, **106**, 447–462.

Gordon, C. T., and W. F. Stern, 1982: A description of the GFDL global spectral model. *Mon. Wea. Rev.*, **110**, 625–644.

Goswami, B. N., and J. Shukla, 1984: Quasi-periodic oscillations in a symmetric general circulation model. *J. Atmos. Sci.*, **41**, 20–37.

Gutzler, D. S., and R. D. Madden, 1989: Seasonal variations in the spatial structure of intraseasonal tropical wind fluctuations. *J. Atmos. Sci.*, **46**, 641–660.

Hayashi, Y., 1970: A theory of large-scale equatorial waves generated by condensational heat and accelerating the zonal wind. *J. Meteor. Soc. Japan*, **48**, 140–160.

——, 1971a: Frictional convergence due to large-scale equatorial waves in a finite-depth Ekman layer. *J. Meteor. Soc. Japan*, **49**, 450–457.

——, 1971b: Large-scale equatorial waves destabilized by convective heating in the presence of surface friction. *J. Meteor. Soc. Japan*, **49**, 458–466.

——, 1971c: Instability of large-scale equatorial waves under the radiation condition. *J. Meteor. Soc. Japan*, **49**, 316–319.

——, 1971d: Instability of large-scale equatorial waves with a frequency-dependent CISK parameter. *J. Meteor. Soc. Japan*, **49**, 59–62.

——, 1974: Spectral analysis of tropical disturbances appearing in a GFDL general circulation model. *J. Atmos. Sci.*, **31**, 180–218.

——, 1976: Non-singular resonance of equatorial waves under the radiation condition. *J. Atmos. Sci.*, **33**, 183–201.

——, 1982: Space–time spectral analysis and its applications to atmospheric waves. *J. Meteor. Soc. Japan*, **60**, 156–171.

——, and D. G. Golder, 1978: The generation of equatorial transient planetary waves: Control experiments with a GFDL general circulation model. *J. Atmos. Sci.*, **35**, 2068–2082.

——, and ——, 1980: The seasonal variation of tropical transient planetary waves appearing in a GFDL general circulation model. *J. Atmos. Sci.*, **37**, 705–716.

——, and ——, 1981: The effects of condensational heating on middle latitude transient waves in their mature stage: Control experiments with a GFDL general circulation model. *J. Atmos. Sci.*, **38**, 2532–2539.

——, and ——, 1986: Tropical intraseasonal oscillations appearing in a GFDL general circulation model and FGGE data, Part I: Phase propagation. *J. Atmos. Sci.*, **43**, 3058–3067.

——, and S. Miyahara, 1987: A three-dimensional linear response model of the tropical intraseasonal oscillation. *J. Meteor. Soc. Japan*, **65**, 843–857.

——, and D. G. Golder, 1988: Tropical intraseasonal oscillations appearing in a GFDL general circulation model and FGGE data. Part II: Structure. *J. Atmos. Sci.*, **45**, 3017–3033.

——, ——, and J. D. Mahlman, 1984: Stratospheric and mesospheric Kelvin waves simulated by the GFDL "SKYHI" general circulation model. *J. Atmos. Sci.*, **41**, 1971–1984.

——, ——, ——, and S. Miyahara, 1989: The effect of horizontal resolution on gravity waves simulated by the GFDL "SKYHI" general circulation model. *Pure Appl. Geophys.*, **130**, 421–443.

Hayashi, Y.-Y., and T. Nakazawa, 1989: Evidence of the existence and eastward motion of superclusters at the equator. *Mon. Wea. Rev.*, **117**, 236–243.

——, and A. Sumi, 1986: The 20–40-day oscillation simulated in an "aqua-planet" model. *J. Meteor. Soc. Japan*, **64**, 431–466.

Hendon, H. H., 1988: A simple model of the 40–50-day oscillation. *J. Atmos. Sci.*, **45**, 569–584.

Hirota, I., 1979: Kelvin waves in the equatorial middle atmosphere observed by the Nimbus 5 SCR. *J. Atmos. Sci.*, **36**, 217–222.

Hollingsworth, A., C. Lorenc, M. S. Tracton, K. Arpe, G. Cats, S. Uppala, and P. Kallberg, 1985: The response of numerical weather prediction systems to FGGE IIb data. Part I: Analyses. *Quart. J. Roy. Meteor. Soc.*, **111**, 1–66.

——, D. B. Shaw, P. Lonnberg, L. Illam, K. Arpe, and A. J. Simmons, 1986: Monitoring of observations and analysis quality by a data assimilation system. *Mon. Wea. Rev.*, **114**, 861–879.

Holton, J. R., 1973: On the frequency distribution of atmospheric Kelvin waves. *J. Atmos. Sci.*, **30**, 499–501.

Hsu, H.-H., B. J. Hoskins, and F. F. Jin, 1990: The 1985/86 intraseasonal oscillation and the role of the extratropics. *J. Atmos. Sci.*, **47**, 823–839.

Itoh, H., 1989: The mechanism for the scale selection of tropical intraseasonal oscillations: Part I: Selection of wavenumber 1 and the three-scale structure. *J. Atmos. Sci.*, **46**, 1779–1798.

——, and N. Nishi, 1990: Consideration for the structure of the tropical intraseasonal oscillation. *J. Meteor. Soc. Japan*, **68**, 659–675.

Kalnay, E., and R. Jenne, 1991: Summary of the NMC/NCAR reanalysis workshop of April 1991. *Bull. Amer. Meteor. Soc.*, **72**, 1897–1904.

Kanamitsu, M., T. N. Krishnamurti, and C. Depradine, 1972: On scale interactions in the tropics during Northern Summer. *J. Atmos. Sci.*, **29**, 698–706.

Keshavamurti, R. N., S. V. Kasture, and V. Krishnakumar, 1986: 30–50-day oscillation of the Monsoon: A new theory. *Beitr. Phys. Atmos.*, **59**, 443–454.

Kinter, J. L., and J. Shukla, 1989: Reanalysis for TOGA (Tropical Oceans, Global Atmosphere). 1–3 February 1989 meeting at the Center for Ocean–Land–Atmosphere Interactions. *Bull. Amer. Meteor. Soc.*, **70**, 1422–1427.

Knutson, T. R., and K. M. Weickmann, 1987: 30–60-day atmospheric oscillations: Composite life cycles of convection and circulation anomalies. *Mon. Wea. Rev.*, **115**, 1407–1436.

——, ——, and J. Steubach, 1986: Global scale intraseasonal oscillations of outgoing longwave radiation and 250-mb zonal wind during Northern Hemisphere summer. *Mon. Wea. Rev.*, **114**, 605–623.

Krishnamurti, T. N., P. K. Jayakumar, J. Sheng, N. Surgi, and A. Kumar, 1985: Divergent circulation on the 30- to 50-day time scale. *J. Atmos. Sci.*, **42**, 364–375.

Kuma, K., 1990a: A quasi-biennial oscillation in the intensity of the intraseasonal oscillation. *Int. J. Climatol.*, **10**, 263–278.

——, 1990b: Diabatic heating and the low frequency dynamics in the tropics. *Meteor. Atmos. Phys.*, **44**, 265–279.

Kuo, H.-L., 1965: On formation and intensification of tropical cyclones through latent heat release by cumulus convection. *J. Atmos. Sci.*, **22**, 40–63.

——, 1975: Instability theory of large-scale disturbances in the tropics. *J. Atmos. Sci.*, **32**, 2229–2245.

Langley, R. G., R. W. King, I. I. Shapiro, R. D. Rosen, and D. A. Salstein, 1981: Atmospheric angular momentum and the length of day: A common fluctuation with a period near 50 days. *Nature*, **294**, 730–732.

Lau, K.-M., and P. H. Chan, 1985: Aspects of the 40–50-day oscillation during the northern winter as inferred from outgoing longwave radiation. *Mon. Wea. Rev.*, **113**, 1889–1909.

——, and ——, 1986a: Aspects of the 40–50 day oscillation during the northern summer as inferred from outgoing longwave radiation. *Mon. Wea. Rev.*, **114**, 1354–1367.

——, and ——, 1986b: The 40–50-day oscillations and the El Niño Southern Oscillation: A new perspective. *Bull. Amer. Meteor. Soc.*, **67**, 533–534.

——, and ——, 1988: Intraseasonal and interannual variations of tropical convection: A possible link between the 40–50-day oscillation and ENSO? *J. Atmos. Sci.*, **45**, 506–521.

——, and H. Lim, 1982: Thermally driven motions in an equatorial beta-plane: Hadley and Walker circulations during the winter monsoon. *Mon. Wea. Rev.*, **110**, 336–353.

——, and L. Peng, 1987: Origin of low frequency (intraseasonal) oscillations in the tropical atmosphere. Part I: Basic theory. *J. Atmos. Sci.*, **44**, 950–972.

——, I.-S. Kang, and P. J. Sheu, 1989: Principal modes of intraseasonal variations in atmospheric angular momentum and tropical convection. *J. Geophys. Res.*, **94**, 6319–6332.

Lau, N.-C., and K.-M. Lau, 1986: The structure and propagation of intraseasonal oscillations appearing in a GFDL GCM. *J. Atmos. Sci.*, **43**, 2023–2047.

——, I. M. Held, and J. D. Neelin, 1988: The Madden–Julian oscillation in an idealized general circulation model. *J. Atmos. Sci.*, **45**, 3810–3932.

Lim, H., T.-K. Lim, and C.-P. Chang, 1990: Reexamination of wave–CISK theory: Existence and properties of nonlinear wave–CISK modes. *J. Atmos. Sci.*, **47**, 3078–3091.

Lindzen, R. S., 1967: Planetary waves on beta planes. *Mon. Wea. Rev.*, **95**, 441–451.

——, 1974: Wave–CISK in the tropics. *J. Atmos. Sci.*, **31**, 156–179.

——, and T. Matsuno, 1968: On the nature of a large-scale wave disturbances in the equatorial stratosphere. *J. Meteor. Soc., Japan*, **46**, 215–221.

Lorenc, A. C., 1984: The evolution of planetary scale 200-mb divergent flow during the FGGE year. *Quart. J. Roy. Meteor. Soc.*, **110**, 427–441.

Madden, R. A., 1979: Observations of large-scale traveling Rossby waves. *Rev. Geophys. Space Phys.*, **17**, 1935–1949.

——, 1986: Seasonal variations of the 40–50-day oscillation in the tropics. *J. Atmos. Sci.*, **43**, 3138–3158.

——, and P. R. Julian, 1971: Detection of a 40–50-day oscillation in the zonal wind in the tropical Pacific. *J. Atmos. Sci.*, **28**, 702–708.

——, and ——, 1972: Description of global-scale circulation cells in the tropics with a 40–50-day period. *J. Atmos. Sci.*, **29**, 1109–1123.

Magana, V., and M. Yanai, 1991: Tropical–midlatitude interaction on the time scale of 30 to 60 days during the northern summer of 1979. *J. Climate*, **4**, 180–201.

Mahlman, J. D., and L. J. Umscheid, 1984: Dynamics of the middle atmosphere: Successes and problems of the GFDL "SKYHI" general circulation models. *Dynamics of the Middle Atmosphere*, J. R. Holton and T. Matsuno, Eds., Terra Scientific, 501–525.

Manabe, S., J. Smagorinsky, and R. F. Strickler, 1965: Simulated climatology of a general circulation model with a hydrologic cycle. *Mon. Wea. Rev.*, **93**, 769–798.

——, D. G. Hahn, and J. L. Holloway, Jr., 1979: Climate simulations with GFDL spectral models of the atmosphere: Effect of truncation. GARP Publ. Ser. No. 22, Vol. 1, 41–94.

Maruyama, T., 1982: Upper tropospheric zonal oscillation with a 30–50-day period over the equatorial western Pacific observed in cloud movement vectors. *J. Meteor. Soc. Japan*, **60**, 172–182.

Matsuno, T., 1966: Quasi-geostrophic motions in the equatorial area. *J. Meteor. Soc. Japan*, **44**, 25–43.

Miyahara, S., 1987: A simple model of the tropical intraseasonal oscillation. *J. Meteor. Soc. Japan*, **65**, 341–351.

Murakami, M., 1979: Large-scale aspects of deep convective activity over the GATE area. *Mon. Wea. Rev.*, **107**, 994–1013.

Murakami, T., 1987: Intraseasonal atmospheric teleconnection patterns during the Northern Hemisphere summer. *Mon. Wea. Rev.*, **115**, 2133–2154.

——, 1988: Intraseasonal atmospheric teleconnection patterns during the Northern Hemisphere winter. *J. Climate*, **1**, 117–131.

——, T. Nakazawa, and J. He, 1984: On the 40–50 day oscillations during the 1979 Northern Hemisphere summer. Part I: Phase propagation. *J. Meteor. Soc. Japan*, **62**, 440–468.

——, ——, and ——, 1984: On the 40–50 day oscillations during the 1979 Northern Hemisphere summer. Part II: Heat and moisture budget. *J. Meteor. Soc. Japan*, **62**, 469–484.

Nakazawa, T., 1986: Intraseasonal variations of OLR in the tropics during the FGGE year. *J. Meteor. Soc. Japan*, **64**, 17–34.

——, 1988: Tropical super clusters within intraseasonal variations over the western Pacific. *J. Meteor. Soc. Japan*, **66**, 823–839.

Neelin, J. D., I. M. Held, and K. H. Cook, 1987: Evaporation–wind feedback and low-frequency variability in the tropical atmosphere. *J. Atmos. Sci.*, **44**, 2341–2348.

Nishi, N., 1989: Observational study on the 30–60-day variations in the geopotential and temperature fields in the equatorial region. *J. Meteor. Soc. Japan*, **67**, 187–203.

Nogués-Paegle, J., B.-C. Lee, and V. E. Kousky, 1989: Observed modal characteristics of the intraseasonal oscillation. *J. Climate*, **2**, 496–507.

Numaguti, A., and Y.-Y. Hayashi, 1991a: Behavior of cumulus activity and the structures of circulations in an "aqua planet" model. Part I: The structure of the super clusters. *J. Meteor. Soc. Japan*, **69**, 541–561.

——, and ——, 1991b: Behavior of cumulus activity and the structures of circulations in an "aqua planet" model. Part II: Eastward-moving planetary scale structure and the intertropical convergence zone. *J. Meteor. Soc. Japan*, **69**, 563–579.

Park, C.-K., D. M. Straus, and K. M. Lau, 1990: An evaluation of the structure of tropical intraseasonal oscillations in three general circulation models. *J. Meteor. Soc. Japan*, **68**, 403–417.

Pitcher, E. J., and J. E. Geisler, 1987: The 40- to 50-day oscillation in a perpetual January simulation with a general circulation model. *J. Geophys. Res.*, **92**, 11 971–11 978.

Salby, M. L., and R. R. Garcia, 1987: Transient response to localized episodic heating in the tropics. Part I: Excitation and short-time near-field behavior. *J. Atmos. Sci.*, **44**, 458–498.

——, D. L. Hartmann, P. L. Bailey, and J. C. Gille, 1984: Evidence for equatorial Kelvin modes in *Nimbus-7* LIMS. *J. Atmos. Sci.*, **41**, 220–235.

Sheng, J., and Y. Hayashi, 1990: Observed and simulated energy cycles in the frequency domain. *J. Atmos. Sci.*, **47**, 1243–1254.

Sui, C.-H., and K.-M. Lau, 1989: Origin of low-frequency (intraseasonal) oscillations in the tropical atmosphere. Part II: Structure and propagation of mobile wave–CISK modes and their modification by lower boundary forcings. *J. Atmos. Sci.*, **46**, 37–56.

Swinbank, R. T., N. Palmer, and M. K. Davey, 1988: Numerical simulations of the Madden and Julian oscillations. *J. Atmos. Sci.*, **45**, 774–788.

Takahashi, M., 1987: A theory of the slow phase speed of the intraseasonal oscillation using the wave–CISK. *J. Meteor. Soc. Japan*, **65**, 43–49.

Tokioka, T., K. Yamazaki, A. Kitoh, and T. Ose, 1988: The equatorial 30–60-day oscillation and the Arakawa–Schubert penetrative cumulus parameterization. *J. Meteor. Soc. Japan*, **66**, 883–901.

Trenberth, K. E., 1984: Interannual variability of the Southern Hemisphere circulation: Representativeness of the year of the global weather experiment. *Mon. Wea. Rev.*, **112**, 108–123.

——, and J. G. Olson, 1988: An evaluation and intercomparison of global analyses from the National Meteorological Center and the European Centre for Medium-Range Weather Forecasts. *Bull. Amer. Meteor. Soc.*, **69**, 1047–1057.

Van Tuyl, A. H., 1987: Nonlinearities in low-frequency equatorial waves. *J. Atmos. Sci.*, **17**, 2478–2492.

Wallace, J. M., and V. E. Kousky, 1968: Observational evidence of Kelvin waves in the tropical stratosphere. *J. Atmos. Sci.*, **25**, 280–292.

Wang, B., 1988: Dynamics of the tropical low-frequency waves. An analysis of the moist Kelvin waves. *J. Atmos. Sci.*, **45**, 2051–2065.

——, and H. Rui, 1990: Dynamics of the coupled moist Kelvin–Rossby wave on an equatorial beta-plane. *J. Atmos. Sci.*, **47**, 397–413.

Webster, P. J., 1983: Mechanism of monsoon low frequency variability: Surface hydrological effects. *J. Atmos. Sci.*, **40**, 2110–2124.

——, and L. C. Chou, 1980: Low frequency transitions of a simple monsoon system. *J. Atmos. Sci.*, **37**, 368–382.

Xie, S.-P., 1991: Evaporation–wind feedback and the organizing of tropical convection on the planetary scale: A theory of tropical intraseasonal oscillations. Ph.D. thesis, Tohoku University, Sendai, Japan, 133 pp.

——, and A. Kubokawa, 1990: On the wave–CISK in the presence of a frictional boundary layer. *J. Meteor. Soc. Japan*, **68**, 651–657.

Yamagata, T., 1987: A simple moist model relevant to the origin of intraseasonal disturbances in the tropics. *J. Meteor. Soc. Japan*, **65**, 153–165.

——, and Y. Hayashi, 1984: A simple diagnostic model for the 30–50-day oscillation in the tropics. *J. Meteor. Soc. Japan*, **62**, 709–717.

Yanai, M., and T. Maruyama, 1966: Stratospheric wave disturbances propagating over the equatorial Pacific. *J. Meteor. Soc. Japan*, **44**, 291–294.

Yano, J.-I., and K. Emanuel, 1991: An improved model of the equatorial troposphere and its coupling with the stratosphere. *J. Atmos. Sci.*, **48**, 377–389.

Yasunari, T., 1981: Structure of an Indian summer monsoon system with around 40-day period. *J. Meteor. Soc. Japan*, **59**, 336–354.

Yoshizaki, M., 1991: Selective amplification of the eastward-propagating mode in a positive-only wave–CISK model on an equatorial beta plane. *J. Meteor. Soc. Japan*, **69**, 353–373.

Zebiak, S. E., 1989: On the 30–60-day oscillation and the prediction of El Niño. *J. Climate*, **2**, 1381–1387.

Zhao, J.-X., and M. Ghil, 1991: Nonlinear symmetric instability and intraseasonal oscillations in the tropical atmosphere. *J. Atmos. Sci.*, **48**, 2552–2568.